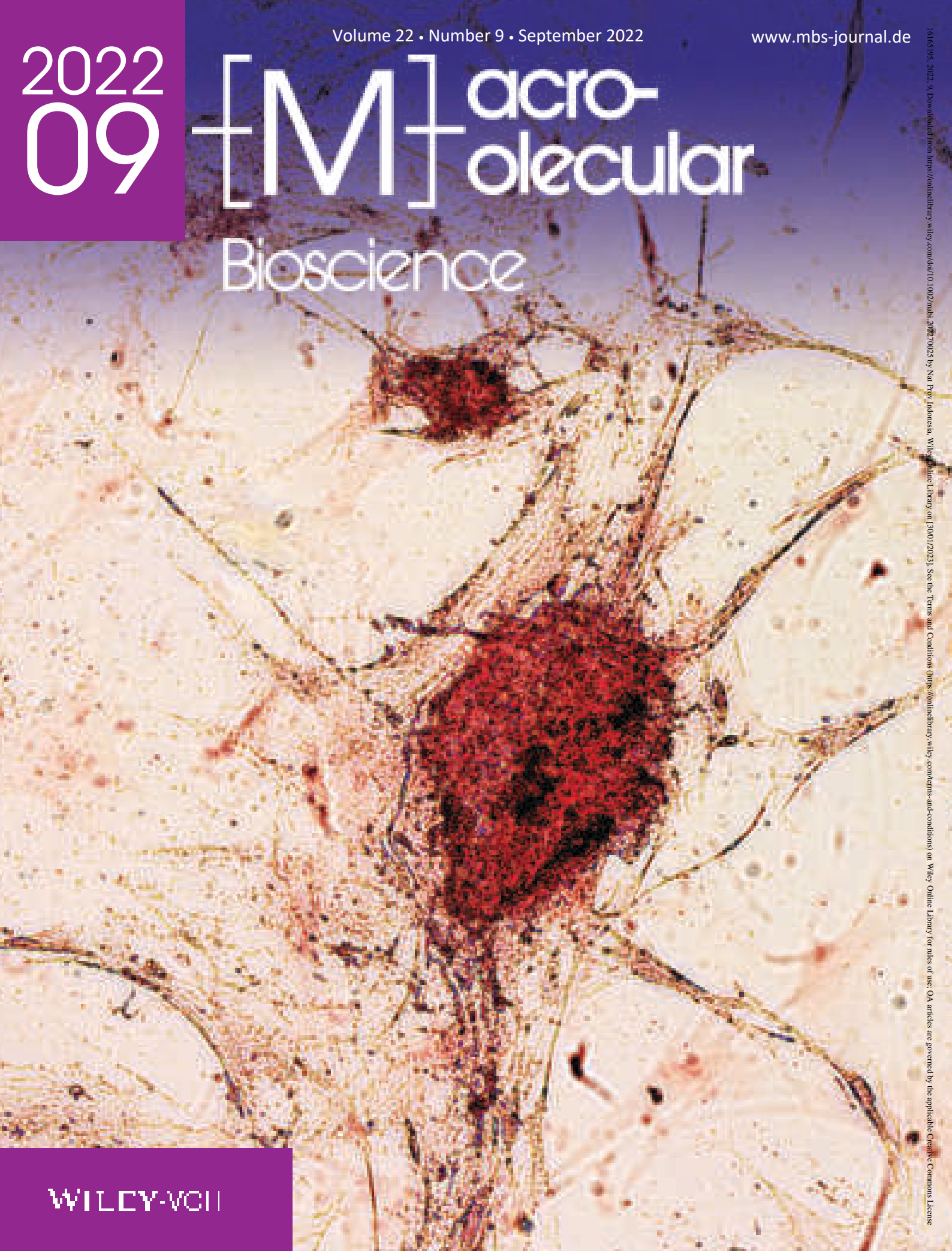


2022
09

[M]acro- molecular Bioscience



WILEY-VCH

Editorial Board

Our journal is managed by professional in-house editors who handle manuscripts from submission to publication and beyond, including overseeing peer review and production steps and liaising with the scientific community. All editors responsible for the peer review process and for editorial decision-making have research backgrounds and hold a PhD. Learn more about our team of professional [in-house editors](#).

Our in-house editors closely collaborate with our Editorial Board Members to ensure the highest publishing standards in accordance with our [editorial policies](#).

Editorial Board Members do not oversee the peer review process.

International Advisory Board *Macromolecular Bioscience*

Matthias Barz, *Leiden University*

Christopher Bettinger, *Carnegie Mellon University, Pittsburgh*

Hans Börner, *Humboldt-University Berlin*

Horacio Cabral, *University of Tokyo*

Xuesi Chen, *Changchun Institute of Applied Chemistry*

Helmut Cölfen, *University of Konstanz*

Timothy J. Deming, *University of California, Los Angeles*

Daidi Fan, *Northwest University, Shaanxi*

Laura Hartmann, *Heinrich-Heine-University Düsseldorf*

Sarah Heilshorn, *Stanford University*

Thomas Heinze, *University of Jena*

David L. Kaplan, *Tufts University, Medford*

Kristi Kiick, *University of Delaware, Newark*

Harm-Anton Klok, *Ecole Polytechnique Fédérale de Lausanne*

Jindřich Kopeček, *University of Utah, Salt Lake City*

Khoon S. Lim, *University of Otago, Dunedin*

Bin Liu, *National University of Singapore **

Robert Luxenhofer, *University of Würzburg*

Heather Maynard, *University of California, Los Angeles*

David J. Mooney, *Harvard University, Cambridge*

Nicholas Peppas, *University of Texas, Austin*

Greg G. Qiao, *University of Melbourne*

Helmut Schlaad, *University of Potsdam*

Martina Stenzel, *University of New South Wales, Sydney*

Nicola Tirelli, *Italian Institute of Technology, Genova*

Jan van Hest, *Radboud University Nijmegen*

Tanja Weil, *Max Planck Institute for Polymer Research, Mainz*

* represents *Macromolecular Bioscience* in the [Wiley Polymer Scientific Advisory Board](#)

Wolfgang P. Meier †, *University of Basel, Switzerland*

Wolfgang P. Meier was formerly a member of the Macromolecular Bioscience International Advisory Board. He will be remembered as an outstanding mentor and as an inspiring and highly creative scientist who was striving the boundaries of chemistry and came up with elegant solutions to important questions in the fields of polymer synthesis and nanoscience. Wolfgang P. Meier has passed away on the 25th of January 2022 after a long illness. In Memoriam Wolfgang P. Meier (1964–2022).

Tools

 [Submit an Article](#)

 [Browse free sample issue](#)

 [Get content alerts](#)

 [Subscribe to this journal](#)

Best of  **acro-**
olecular Journals

Best of Macros 2021/22 is now online. Click [here](#) to read the articles selected this year.

Volume 22, Issue 9

September 2022

< Previous Issue | Next Issue >

☰ GO TO SECTION

🗉 Export Citation(s)

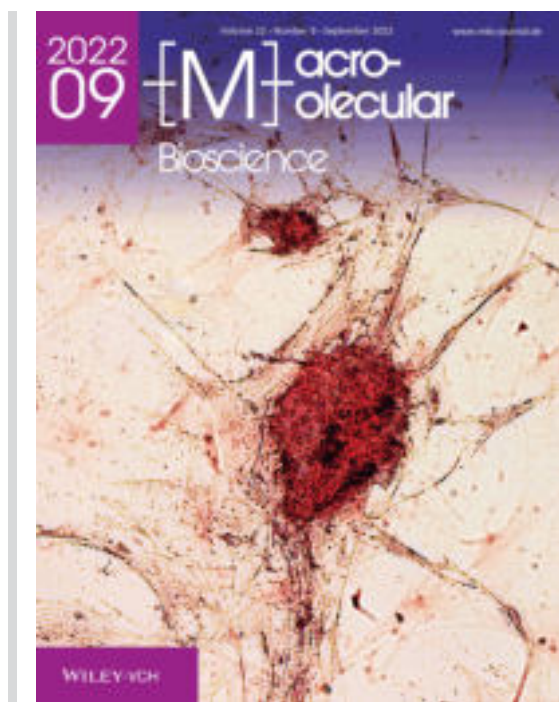
Cover Picture

🔓 Free Access

Nanoarchitectonics of Fullerene-Based Enzyme Mimics for Osteogenic Induction of Stem Cells

Dilara Yeniterzi, Zeynep Demirsoy, Aytül Saylam, Salih Özçubukçu, Gülcihan Gülseren

First Published: 14 September 2022



Front Cover: Fullerene nanoparticles decorated with histidine and serine amino acids, which are the elements of catalytic triad, imitates the phosphatase class of enzymes by cleaving phosphate groups from various molecules. When these nanocatalysts are applied to preosteoblast and mesenchymal stem cells, they cause the differentiation of these cells into osteoblasts by changing the gene expression patterns and increasing biomineralization. This is reported by Gülcihan Gülseren and co-workers in article number [2200079](#).

[Abstract](#) | [PDF](#) | [Request permissions](#)

Masthead

[Free Access](#)**Masthead: Macromol. Biosci. 9/2022**

First Published: 14 September 2022

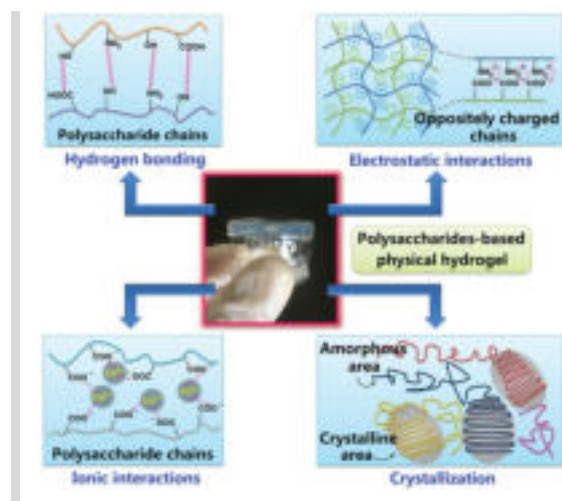
[PDF](#) | [Request permissions](#)

Reviews

Recent Advances in Polysaccharide-Based Physical Hydrogels and Their Potential Applications for Biomedical and Wastewater Treatment

Xinyu Hu, Liangliang Zhang, Linlin Yan, Lihua Tang

First Published: 18 May 2022



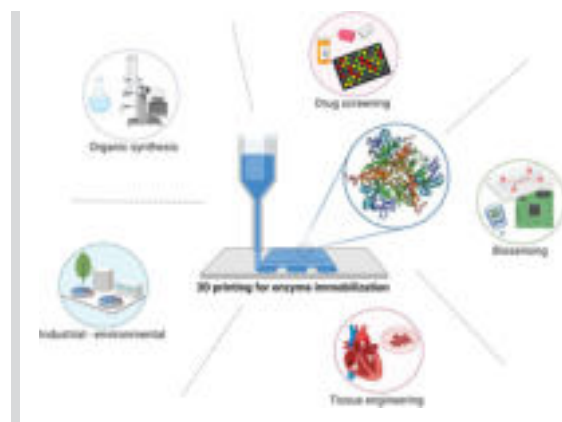
This review describes the noncovalent interactions between the functional groups of polysaccharide chains, such as hydrogen bonding, electrostatic interactions, ionic interactions, and crystallization. The crosslinked polysaccharide networks are generated in a simple, reliable, and environmental-friendly way, and the final structure of gel network is thus stabilized by these noncovalent interactions.

[Abstract](#) | [Full text](#) | [PDF](#) | [References](#) | [Request permissions](#)[Open Access](#)

3D Printing: An Emerging Technology for Biocatalyst Immobilization

Tomás Pose-Boirazian, Jose Martínez-Costas, Gemma Eibes

First Published: 17 May 2022



This review presents an overview of the onset of 3-dimensional printing (3DP) in the field of enzyme immobilization. Examples of the latest 3D printed enzyme-immobilized industrial and clinical applications are shown. The unique advantages of enzymatic 3D printing are also discussed, alongside its potential limitations and the future perspectives.

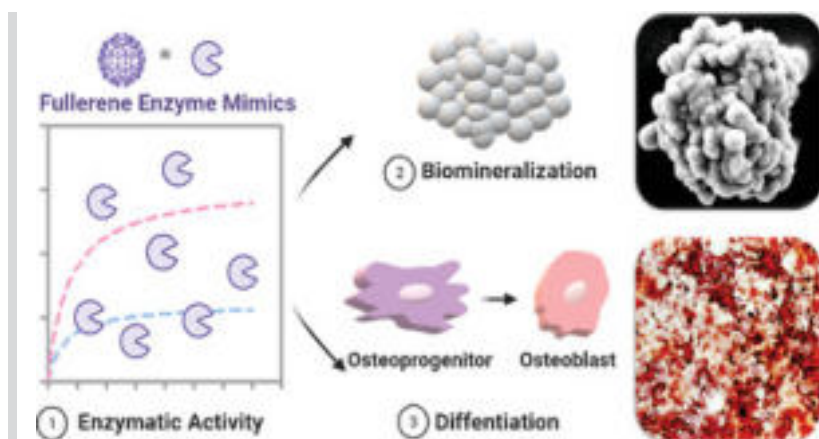
[Abstract](#) | [Full text](#) | [PDF](#) | [References](#) | [Request permissions](#)

Research Articles

Nanoarchitectonics of Fullerene-Based Enzyme Mimics for Osteogenic Induction of Stem Cells

Dilara Yeniterzi, Zeynep Demirsoy, Aytül Saylam, Salih Özçubukçu, Gülcihan Gülseren

First Published: 25 June 2022



In this study, a simple module for mimicking various functions and features of phosphatase enzyme is developed. The approach uses fullerene nanocages, as a scaffold that is functionalized to perform rapid catalysis, biomineralization, and stem cell differentiation at the same time.

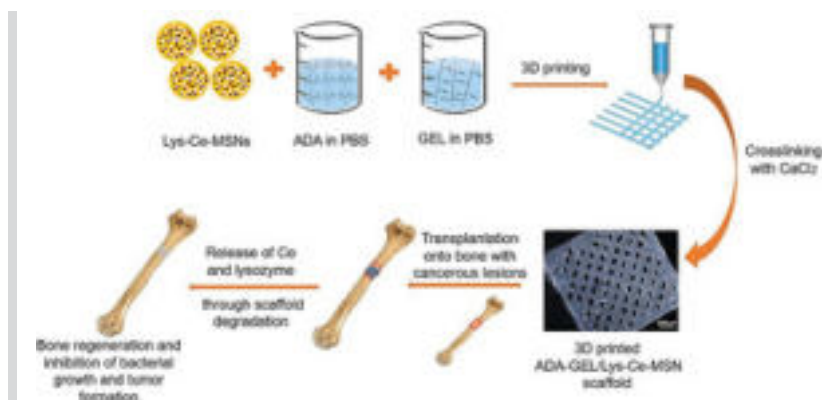
[Abstract](#) | [Full text](#) | [PDF](#) | [References](#) | [Request permissions](#)

[Open Access](#)

A 3D Printed Bone Tissue Engineering Scaffold Composed of Alginate Dialdehyde-Gelatine Reinforced by Lysozyme Loaded Cerium Doped Mesoporous Silica-Calcia Nanoparticles

Mahshid Monavari, Rucha Medhekar, Qaisar Nawaz, Mehran Monavari, Miguel Fuentes-Chandía, Shahin Homaeigohar, Aldo R. Boccaccini

First Published: 06 July 2022



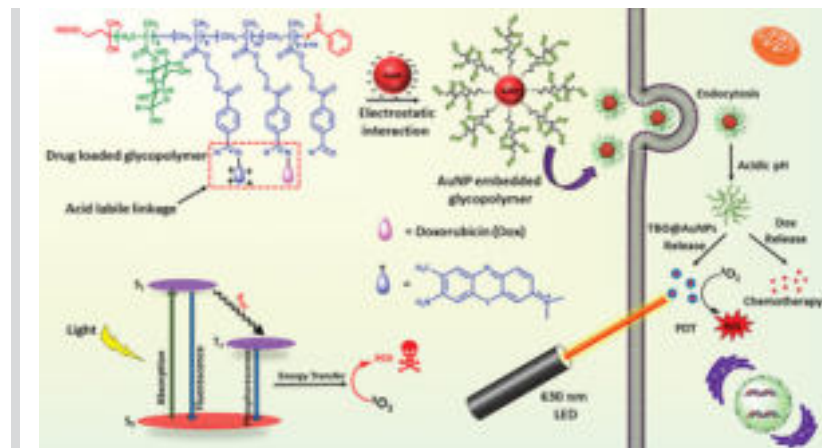
Alginate dialdehyde-gelatine (ADA-GEL) hydrogel augmented by lysozyme (Lys) loaded mesoporous cerium doped silica-calcia nanoparticles (Lys-Ce-MSNs) are 3D printed to develop a new family of bioactive scaffolds with mineralization capability. The scaffolds deliver biologically active ions and Lys to achieve antibacterial (and potentially anticancer) properties. In combination with gentamicin, Lys induces antibacterial efficiency against gram-positive and gram-negative bacteria.

[Abstract](#) | [Full text](#) | [PDF](#) | [References](#) | [Request permissions](#)

Gold Nanoparticle Embedded Stimuli-Responsive Functional Glycopolymer: A Potential Material for Synergistic Chemo-Photodynamic Therapy of Cancer Cells

Koushik Bhattacharya, Subhayan Das, Moumita Kundu, Sudarshan Singh, Uddhab Kalita, Mahitosh Mandal, Nikhil K. Singha

First Published: 07 July 2022



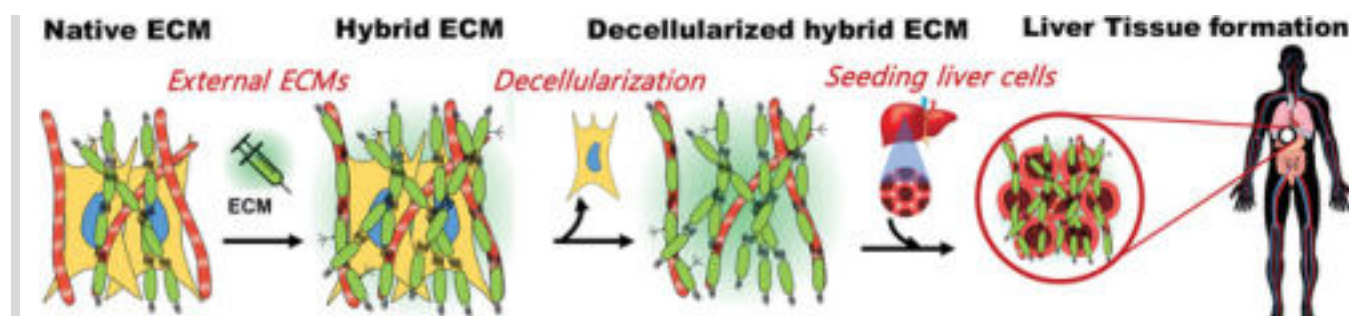
This work describes the fabrication of gold nanoparticles (AuNPs) embedded stimuli-responsive glycopolymer for the efficient treatment of cancer via the synergistic effect of photodynamic therapy and chemotherapy. The efficacy of this hybrid platform is studied over MDA MB 231, human breast cancer cell line.

[Abstract](#) | [Full text](#) | [PDF](#) | [References](#) | [Request permissions](#)

Fabrication of a Tailored, Hybrid Extracellular Matrix Composite

Agustina Setiawati, Sungwoo Jeong, Albertus Ivan Brilian, Sang Ho Lee, Jin-Gon Shim, Kwang-Hwan Jung, Kwanwoo Shin

First Published: 28 June 2022



A native extracellular matrix (ECM) produced by skin fibroblasts is complexed with externally supplied ECM proteins such as fibronectin (FN) and collagen I (COL I), and then transformed into a tailored composite ECM scaffold, a liver tissue resembling FN-rich ECM. This approach is promising to produce of scaffolds providing a tailored cellular microenvironment to specific organs and serving novel pathways for tissue regeneration.

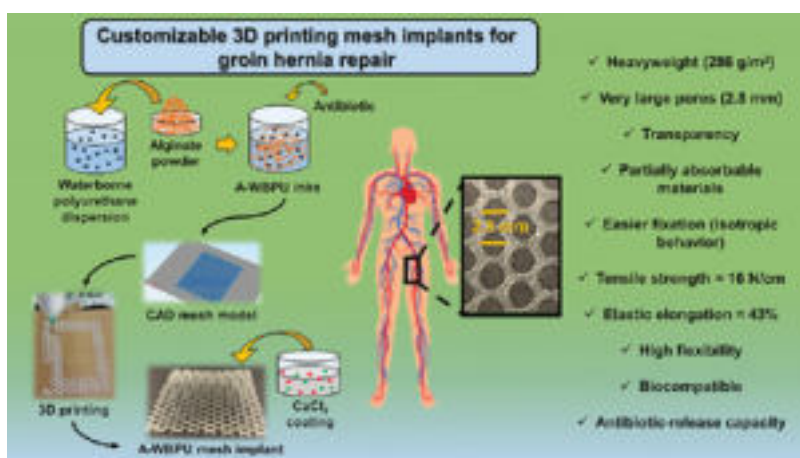
[Abstract](#) | [Full text](#) | [PDF](#) | [References](#) | [Request permissions](#)

[Open Access](#)

Tailor-Made 3D Printed Meshes of Alginate-Waterborne Polyurethane as Suitable Implants for Hernia Repair

Raquel Olmos-Juste, Sheila Olza, Nagore Gabilondo, Arantxa Eceiza

First Published: 29 June 2022



Alginate-waterborne polyurethane (A-WBPU) ink formulations are developed for 3D printing. 3D printed A-WBPU mesh implants present proper morphological characteristics. A CaCl_2 coating provides physical and mechanical reinforcement of the A-WBPU meshes. Mesh with higher alginate content is the best to support physiological corporal movements. Chloramphenicol-loaded 3D printing meshes release antibiotic during the first 24 h.

[Abstract](#) | [Full text](#) | [PDF](#) | [References](#) | [Request permissions](#)

Polyelectrolyte Complex Hydrogels with Controlled Mechanics Affect Mesenchymal Stem Cell Differentiation Relevant to Growth Plate Injuries

Michael A. Stager, Stacey M. Thomas, Nicholas Rotello-Kuri, Karin A. Payne, Melissa D. Krebs

First Published: 14 July 2022

In the presented work, polyelectrolyte complex hydrogels are fabricated using alginate and chitosan. The hydrogels exhibit excellent control over their stiffness, and they affect human mesenchymal stem cell differentiation *in vitro*. The hydrogels are employed in a rat growth plate injury model and show promise as an injectable biomaterial for growth plate injuries.

[Abstract](#) | [Full text](#) | [PDF](#) | [References](#) | [Request permissions](#)

[Open Access](#)

Exploiting Meltable Protein Hydrogels to Encapsulate and Culture Cells in 3D

Gema Dura, Maria Crespo-Cuadrado, Helen Waller, Daniel T. Peters, Ana Ferreira-Duarte, Jeremy H. Lakey, David A. Fulton

First Published: 03 July 2022

Just melt, cool and add cells! Cells are encapsulated within a chemically crosslinked hydrogel that exploits the meltable feature of the protein polymer capsular antigen fragment 1. This approach avoids the need for potentially cytotoxic or costly chemical crosslinking chemistries and can be used to encapsulate even relatively high cell densities.

[Abstract](#) | [Full text](#) | [PDF](#) | [References](#) | [Request permissions](#)

3D Contour Printing of Anatomically Mimetic Cartilage Grafts with Microfiber-Reinforced Double-Network Bioink

Meng Wang, Jianping Zhao, Yixuan Luo, Qianyi Liang, Yisi Liu, Gang Zhong, Yin Yu, Fei Chen

First Published: 07 July 2022

Here, 3D printing of short fiber-reinforced double-network bioink to generate anatomically accurate and mechanical tunable scaffold for cartilage regeneration is reported. The incorporation of poly(lactic acid) short fibers not only improves the printing fidelity but also facilitates the generation of mechanically strong constructs.

[Abstract](#) | [Full text](#) | [PDF](#) | [References](#) | [Request permissions](#)

 [Open Access](#)

New Gelatin-Based Hydrogel Foams for Improved Substrate Conversion of Immobilized Horseradish Peroxidase

Friederike Dehli, Cosima Stubenrauch, Alexander Southan

First Published: 01 July 2022

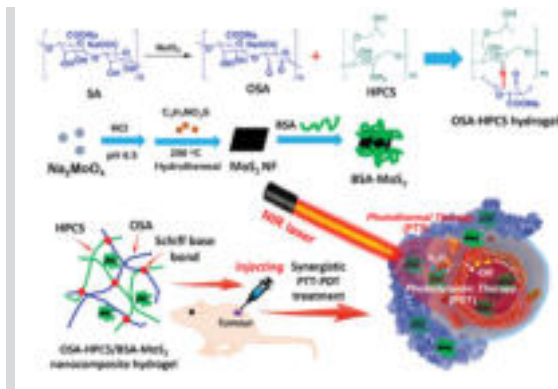
To immobilize streptavidin-conjugated enzymes on gelatin-based hydrogels, a new biotinylated gelatin derivative (GM10EB) is synthesized, which is used to prepare both foamed and nonfoamed hydrogels. When assessing the rate of substrate conversion of enzymes immobilized in foamed and nonfoamed hydrogels, a 12 times increased rate is found for foamed hydrogels.

[Abstract](#) | [Full text](#) | [PDF](#) | [References](#) | [Request permissions](#)

Injectable and Self-Healing Polysaccharide Hydrogel Loading Molybdenum Disulfide Nanoflakes for Synergistic Photothermal-Photodynamic Therapy of Breast Cancer

Yujie Qi, Yifeng Yuan, Zhiyi Qian, Xiaodie Ma, Weizhong Yuan, Ye Song

First Published: 08 June 2022



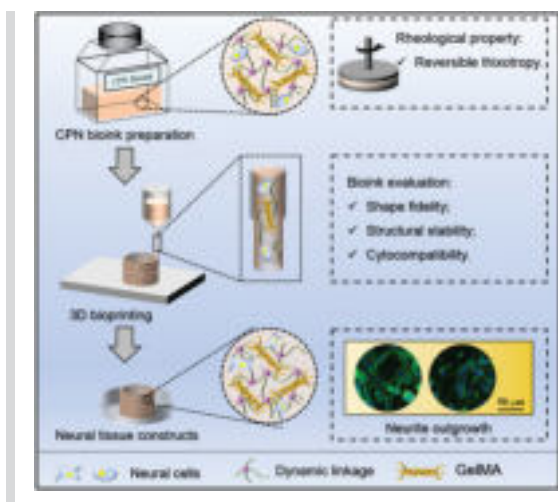
The injectable and self-healing hydrogel is prepared by the Schiff base bonds formed between the aldehyde groups of oxidized sodium alginate and the amino groups of hydroxypropyl chitosan. The nanocomposite hydrogel loading molybdenum disulfide nanoflakes (MoS₂ NFs) can be injected directly to the site of breast cancer. The nanocomposite hydrogel can achieve the accurate and synergistic photothermal-photodynamic therapy of tumors.

[Abstract](#) | [Full text](#) | [PDF](#) | [References](#) | [Request permissions](#)

Development and Characterization of Complementary Polymer Network Bioinks for 3D Bioprinting of Soft Tissue Constructs

Shaoshuai Song, Yuxuan Li, Jie Huang, Zhijun Zhang

First Published: 01 July 2022



A novel strategy for the utilization of complementary polymer network bioinks with reversible thixotropy is established for the manufacture of neural tissue constructs

[Abstract](#) | [Full text](#) | [PDF](#) | [References](#) | [Request permissions](#)

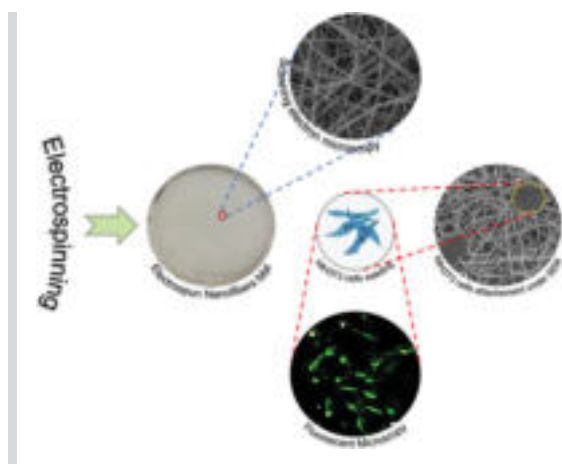
[Open Access](#)

Electrospun Antibacterial Composites for Cartilage Tissue Engineering

Muhammad Samie, Ather Farooq Khan, John George Hardy, Muhammad Arfat Yameen

First Published: 18 July 2022

Electrospinning is used to produce mats of nonwoven nanoscale fibers composed of degradable polymers and optionally an antibiotic medication (cefixime). The mats have mechanical properties analogous to cartilage tissue and are capable of the controlled release of the cefixime. Such materials have potential for implantable pharmaceutical delivery to soft tissues and cartilage tissues.

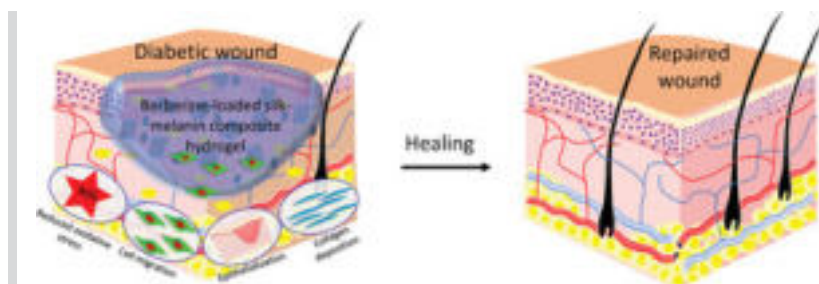


[Abstract](#) | [Full text](#) | [PDF](#) | [References](#) | [Request permissions](#)

Antioxidant Silk Fibroin Composite Hydrogel for Rapid Healing of Diabetic Wound

Biswanath Maity, Shadab Alam, Sourav Samanta, Relekar G. Prakash, Thimmaiah Govindaraju

First Published: 03 August 2022



A composite hydrogel formulation of natural constituents, hypolipidemic silk fibroin, melanin and berberine is reported to tackle various physiological abnormality associated with diabetic wound healing. The biocompatible composite hydrogel effects rapid wound healing by promoting cell migration, reduction of reactive species, enhanced tissue re-epithelialization and collagen deposition in type I diabetic model.

[Abstract](#) | [Full text](#) | [PDF](#) | [References](#) | [Request permissions](#)

Tools

[Submit an Article](#)

[Browse free sample issue](#)

 Get content alerts Subscribe to this journal

Best of **[M]**acromolecular Journals

Best of Macros 2021/22 is now online. Click [here](#) to read the articles selected this year.

Tweets from @AdvSciNews

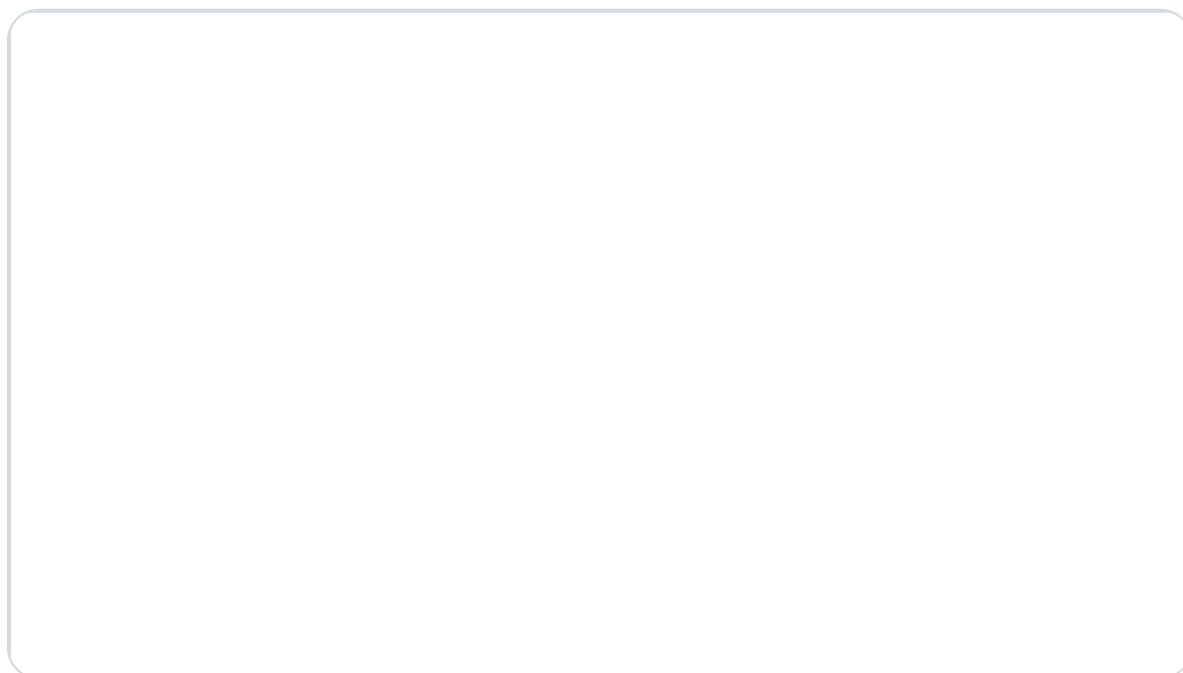
[Follow on Twitter](#)

Advanced Sci News @AdvSciNews · 35m 

This video showcases a design strategy devised to make microporous structures using melt electrowriting.

The approach uses an algorithm that creates arrays of parallel fibers arranged to build channel-like pores.

Read the paper: ow.ly/IGo650MEj0k



Related Titles

- [Macromolecular Rapid Communications](#)

- Macromolecular Chemistry and Physics
- Macromolecular Materials and Engineering
- Macromolecular Theory and Simulations
- Macromolecular Reaction Engineering
- Journal of Polymer Science
- Journal of Applied Polymer Science
- Advanced Healthcare Materials
- Biopolymers
- Peptide Science

DIVERSITY

in Research Jobs

Please [contact us](#) to see your job listed here

[More jobs](#) ►

About Wiley Online Library

[Privacy Policy](#)

[Terms of Use](#)

[About Cookies](#)

[Manage Cookies](#)

[Accessibility](#)

[Wiley Research DE&I Statement and Publishing Policies](#)

[Developing World Access](#)

[Help & Support](#)

Contact Us
Training and Support
DMCA & Reporting Piracy
Opportunities

Subscription Agents
Advertisers & Corporate Partners

Connect with Wiley

The Wiley Network
Wiley Press Room

Copyright © 1999-2023 John Wiley & Sons, Inc. All rights reserved

WILEY

Fabrication of a Tailored, Hybrid Extracellular Matrix Composite

Agustina Setiawati, Sungwoo Jeong, Albertus Ivan Brilian, Sang Ho Lee, Jin-Gon Shim, Kwang-Hwan Jung, and Kwanwoo Shin*

The extracellular matrix (ECM) is a network of connective fibers that supports cells living in their surroundings. Native ECM, generated by the secretory products of each tissue's resident cells, has a unique architecture with different protein composition depending on the tissue. Therefore, it is very difficult to artificially design *in vivo* architecture in tissue engineering. In this study, a hybrid ECM scaffold from the basic structure of fibroblast-derived cellular ECMs is fabricated by adding major ECM components of fibronectin (FN) and collagen (COL I) externally. It is confirmed that while maintaining the basic structure of the native ECM, major protein components can be regulated. Then, decellularization is performed to prepare hybrid ECM scaffolds with various protein compositions and it is demonstrated that a liver-mimicking fibronectin (FN)-rich hybrid ECM promoted successful settling of H4IIE rat hepatoma cells. The authors believe that their method holds promise for the fabrication of scaffolds that provide a tailored cellular microenvironment for specific organs and serve as novel pathways for the replacement or regeneration of specific organ tissues.

(FN) present in the formed tissue, are continuously replaced and rebuilt by the cells residing in the tissue.^[2-4] Thus, the chemical content and topology of a particular ECM in a tissue are known to determine the behavior and the fate of the cells surrounded by that ECM. For example, during myocardial infarction, alterations in the ECM composition induce the activation of fibroblasts and the transdifferentiation of myofibroblasts.^[5-7] The combination of specific ECMs also promotes the differentiation of stem cells into cardiomyocytes or endothelial cells.^[8] In addition to its composition, the topography of the scaffold dictates the way in which tendon stem cells develop into a tendon lineage.^[9] As a result, the ECM is considered an ideal scaffold material in nature, and studies to manipulate the chemical composition and topography of ECM scaffolds to promote the repair or regeneration of

1. Introduction

That the signaling pathways of the surrounding microenvironment, particularly the extracellular matrix (ECM), regulate cellular phenotypes and molecular activities has been well established.^[1] The ECM is composed of a specific combination of the proteins constituting the specific tissue in an organ, and the major ECM components, such as collagen (COL) and fibronectin

damaged organs in tissue engineering are becoming increasingly significant.

Two types of bioscaffolds are frequently used in tissue engineering, depending on the source of the ECM: a native and an artificially constructed ECM scaffold. To begin, the native ECM scaffold contains functional and structural molecules that are organized in a unique 3D structure generated by the secretory products of each tissue's resident cells and are often retrieved through decellularization of tissues or whole organs.^[10,11] Due to the fact that the native ECM is naturally constructed, it has a complex composition with many heterogeneous tissue-specific components.^[12] As a result, the native ECM promotes tissue regeneration via recellularization of the same or a similar tissue source, making it an ideal platform for organ replacement and tissue repopulation.^[13,14] From this point of view, the most successful approach currently employed in regenerative medicine is autografting cells, tissues, or protein scaffolds with minimal immunological complications.^[15] Allografts and xenografts, on the other hand, have potential ethical and immunological issues that limit transplant therapy as a medical treatment option.^[16,17] Due to the composition and the architectural complexity of native ECM, the use of a single or a few components in the fabrication of tissue scaffolds cannot fully recapitulate its properties, restricting the production of a standardized structure composed of identical components or a universally applicable scaffold. Our study developed a new method for transforming the architecture

A. Setiawati, S. Jeong, A. I. Brilian, S. H. Lee, K. Shin
 Department of Chemistry and Institute of Biological Interfaces
 Sogang University
 35 Baekbeom-ro
 Mapo-gu, Seoul 04107, Republic of Korea
 E-mail: kwshin@sogang.ac.kr

A. Setiawati, J.-G. Shim, K.-H. Jung
 Department of Life Science
 Sogang University
 35 Baekbeom-ro
 Mapo-gu, Seoul 04107, Republic of Korea

A. Setiawati
 Faculty of Pharmacy
 Sanata Dharma University
 Paingan, Maguwoharjo, Depok
 Sleman, Yogyakarta 55281, Indonesia

 The ORCID identification number(s) for the author(s) of this article can be found under <https://doi.org/10.1002/mabi.202200106>

DOI: 10.1002/mabi.202200106

of native tissue obtained from living tissue into an implantable scaffold engineered from a single cell type (i.e., fibroblast) to be transferable to various scaffolds, which can be applicable to multiple tissues and organs.

In contrast to native ECM, which is created through cellular fibrillogenesis, an artificial ECM scaffold can be engineered by artificially complexing isolated protein molecules or externally expressed proteins.^[18] While their detailed functions are not ideal in comparison to tissue-derived ECMs, they have the advantage of being able to use the same engineering protocols to mass produce the required ECM components and structures.^[12] In this regard, native and artificial ECM scaffolds each have their own set of advantages and disadvantages. Therefore, the need for such an artificial ECM has been demonstrated in various studies, aiming to replace the native ECM; tunable artificial ECMs have been created by adding biomimetic integrin binding peptides like GFOGER in collagen, arginine-glycine-aspartate (RGDs) in fibronectin, or growth factors to synthetic or naturally derived polymers for tissue engineering, regeneration, or drug screening.^[19–23] Synthetic or natural polymer-based cell culture systems have been successfully designed to sufficiently approximate controllable and complex microenvironments; tunable fabrication, long-term mechanical stability, and reproducibility of each batch remain challenging.^[24] While the composition and the structure of native ECMs need to be further understood and elucidated, artificial ECM scaffolds need to be further manipulated to mimic the same microenvironment as tissue-derived ECMs.

Cryptic units are often found in ECM proteins that either promote autonomous fibrinogenesis or stimulate the binding of other proteins in the vicinity.^[25] In particular, FN plays an important role in extracellular matrix assembly due to its ability to undergo fibrinogenesis to form FN fibrils (FNfs) and to recruit various ECM molecules such as collagen, heparin, and chondroitin sulfate.^[26] Using denaturants and reducing agents, as well as negative charges on the surface, cell-free FN networks have been engineered to open the cryptic domains of human plasma FN.^[18,27–29] In a prior study, we demonstrated complex ECM protein fibrils in which components like FN, collagen, and laminin are integrated relying on these characteristics.^[18,25] Multicomponent ECM hybridization could be built on the interlay of binding domains with fibril formation.^[25,30,31] On the other hand, in 2021 Neale et al. demonstrated that shear-deployed FNfs could successfully induce an ordered and robust 3D network of FNfs, which can then be used to promote a directional, persistent migratory phenotype in fibroblasts.^[32] Despite certain *in vivo* mimetic fibril structures and component hybridizations, they have yet to achieve the biologically complex structures and component configurations produced by the resident cells in a specific tissue. Therefore, it remains an important challenge to produce a tailored ECM scaffold that resembles native ECM through a simple and facile fabrication method.

2. Result and Discussion

2.1. FN Fibrillogenesis on Micropatterned Fibroblasts

Herein, we demonstrate a hybrid ECM scaffold made of a desired composition by complexing externally supplied protein

components using the native architecture of ECM derived from living cells as a template. Based on a proteomic study by Goddard et al.,^[33] the mouse mammary gland and liver had quite different ECM compositions as detailed in Tables S1 and S2, Supporting Information; more than 90% of the ECM component of the rat mammary gland is composed of collagen derivatives, whereas only 0.66% of the ECM component is FN (Table S1, Supporting Information). In another model of the rat liver (Table S2, Supporting Information), the total composition of collagen derivatives was greatly reduced, while the composition of FN surged to 6.01%, about ten times that of the rat mammary gland. Therefore, as a contrasting conceptual model, hybrid ECMs with components at both extremes (COL I-rich and FN-rich ECMs, respectively) were designed as an example of selectively varying the composition of FN or COL I. As schematically depicted in **Figure 1a**, a native ECM produced by skin fibroblasts was complexed with externally supplied ECM proteins such as FN and COL I, and then transformed into composite ECM scaffolds, either a liver tissue resembling FN-rich ECM or a breast tissue resembling COL I-rich ECM. We believe that our approach is promising for the production of scaffolds that provide a tailored cellular microenvironment to specific organs and ultimately serve as novel pathways for tissue engineering that can replace or regenerate specific organ tissues.

FN was first micropatterned on chemically surface-activated PDMS by using (3-aminopropyl) triethoxysilane and glutaraldehyde,^[34] as shown in **Figure 1b**. All cell experiments in this study used the same 50 μm thick line and gap pattern. This strategy was a highly reproducible method of stamping FNs and, more importantly, induces globular FNs into an unfolded state, which promotes fibroblast adherence in a longitudinally directed manner while also stimulating ECM formation on the adsorbed cells.^[35–37] The RGD sequence of the FN type III domain exposed to the unfolded FN molecule by microcontact printing (μCP) binds to the cell through the $\alpha_5\beta_1$ integrin receptor. It is known that the adsorbed cells form a focal adhesion (FA) complex composed of vinculin, actin, actinin, FA kinase (FAK), etc., interacting with cytoskeletal actin to regulate mechanical transformation and FA dynamic turnover.^[38–40] Then, those fibroblasts adsorbed to the micropatterns grew in the longitudinal direction and developed into tissues through intercellular tight junctions with surrounding cells, proceeding with cellular FN fibrillogenesis. In the absence of cells, it was confirmed that red fluorescent plasma FNs (pFN) were adsorbed to the FN pattern (FNp) without forming fibrils, as shown in **Figure 1c**. On the other hand, cells adsorbed to micropatterned FNs produce cellular FN (cFN) fibrils parallel to the cellular orientation, as shown in **Figure 1d**. Interestingly, longitudinally oriented yellow fibers were clearly identified, and it is understood that the exposed cryptic FN-binding sites of cFN recruited pFN as externally provided red pFNs complexed with green FNfs around the cells. As a result, thick fiber complexes with pFN formed around the cell, which we now refer to as hybrid FN fibers.

As the fibroblasts spread and align on the micropattern, they deposit ECM fibrils, containing cFN and COL I, denoted by COL IA1, generating a native ECM network. **Figure 1e** shows representative native ECMs generated by the fibroblasts adsorbed onto a non-fluorescent FN micropattern. When compared with

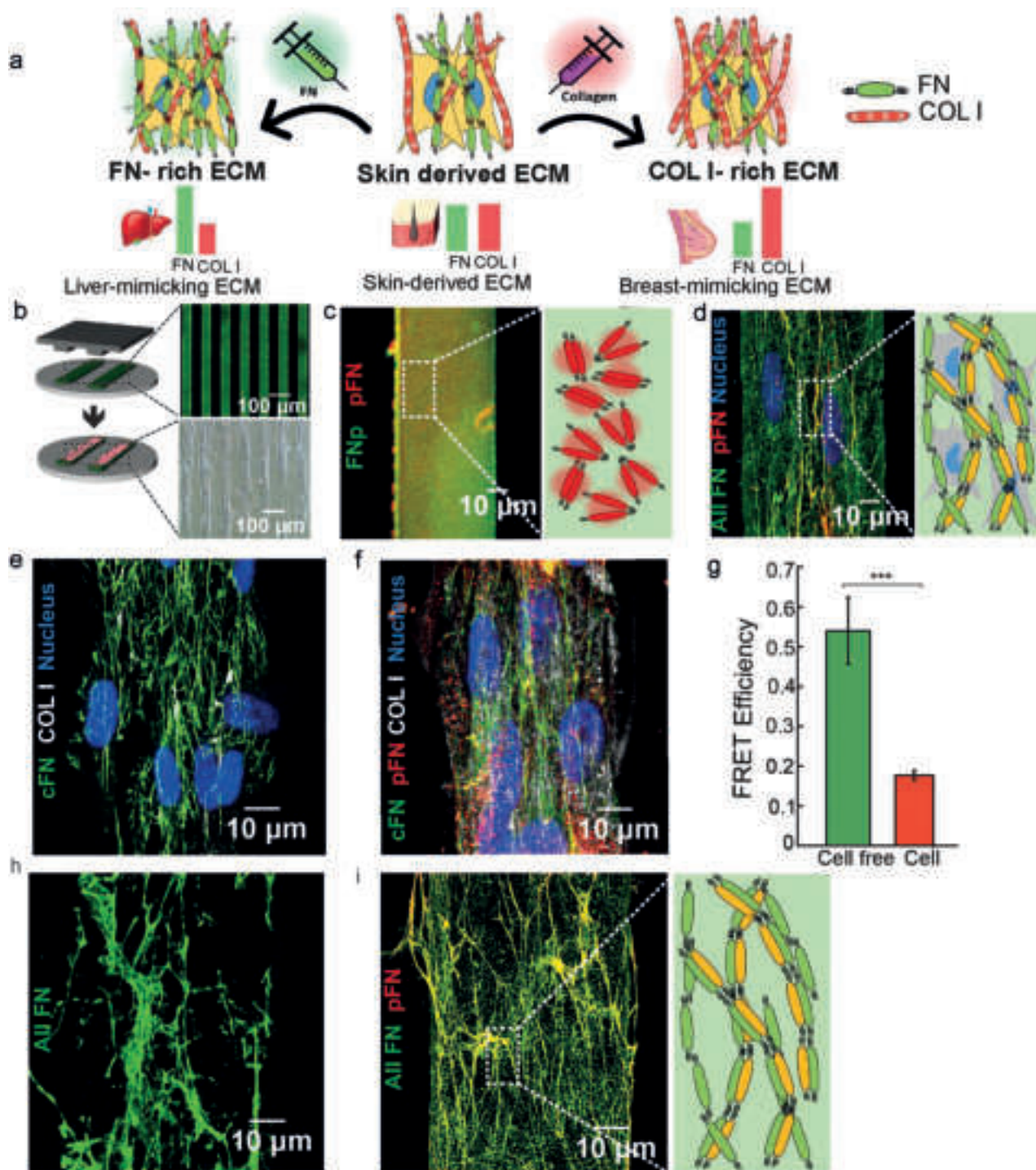


Figure 1. Fibronectin fibrillogenesis on micropatterned fibroblasts. a) Scheme illustrating the fabrication of a tailored-ECM composite to resemble a liver FN-rich ECM or a breast tissue resembling COL I-rich ECM from the native ECM produced from skin fibroblasts by externally supplied ECM proteins such as FN and COL I. b) Illustrations of micro-contact printing of the FN pattern (FNp) and the seeded fibroblasts (left), and confocal and light microscope images (right) of these illustrations. c) A confocal image of pFN deposited on a cell-free FNp on the left, with an illustration of the globular pFN (red) adsorbed on the FNp (green) on the right. d) On the left, a confocal image of pFN deposited on a cell seeded with FNp, and on the right, an illustration of the yellow-colored fibrils generated when pFN (red) hybridized with cFN (green). e, f) Confocal images of FN and COL I networks obtained from e) fibroblasts grown on a non-fluorescent FN micropattern and f) fibroblasts after having added pFN (red). g) The fluorescence resonance energy transfer (FRET) efficiency was calculated with Leica LASX software; data are means \pm standard deviations (SDs) for $n = 5$ experiments. Statistical significance was determined using a one-way ANOVA followed by the Tukey test; $***p < 0.001$. h, i) Confocal images of FN and COL I networks obtained from h) the decellularized native ECM patterns and i) the decellularized, hybrid network. The yellow-colored fibrils were generated when red-colored pFNs were merged with green-colored cFN, as illustrated in a model on the right.

Figure 1d, in which the green fluorescent background and fibrils coexist, it can be confirmed that all green FNs only appear in the form of fine fibrils. Figure 1f shows that when red fluorescent pFN and COL I were added to the native ECM-formed cells, the native ECM was transformed into a much more complex hybrid ECM; yellow hybrid fibers were newly formed; nonfibrillated pFNs islands adsorbed to the micropatterned FNs on the bottom were scattered; in addition, increased COL I molecules (white) were observed. Although COL I polymerization can occur indirectly via $\alpha 5 \beta 1$ integrin and direct collagen-binding integrin, what is noteworthy in this study is that FN fibrils may act as modulators of fibrillar COL I nucleation as an initiating step in polymerization.^[41–43]

When fibrils are being formed, the FN molecule must transform from a soluble, dense state to an insoluble, expanded form. Thus, we wanted to determine whether the globular pFN coupled to the native ECM was then denatured to form a fibrillar FN. In Figure 1g, fluorescence resonance energy transfer (FRET) was used to identify conformational changes in FNs during network formation. As a control, FN adsorbed to the cell-free pattern of Figure 1c was compared. Densely folded FNs with donor and acceptor in close proximity exhibited strong energy transfer with a FRET efficiency of 0.81 ± 0.10 , whereas in 4- and 6-m Gdn HCl, leading to fully unfolded denaturation of 0.14 ± 0.03 and 0.137 ± 0.01 , respectively (Figure S1a, Supporting Information). The FRET efficiency was measured based on an acceptor photobleaching method. After photobleaching, the donor intensity did not increase very much in the cell experiment while it visually increased in the cell-free group (Figure S1b,c, Supporting Information). The increase of donor intensity after acceptor photobleaching indicated higher FRET efficiency. When pFN was deposited on the FN micropattern, a FRET efficiency of 0.54 ± 0.09 was measured, which is thought to be that the pFNs were partially opened by the extended FN molecules mechanically by μ CP.^[44] However, when pFNs are deposited on cell-induced FNfs (as shown in Figure 1g), the FRET efficiency drops sharply to 0.17 ± 0.01 ($**p < 0.001$). These results show that pFN molecules induced by cFN fibrils were denatured into a form similar to cell-derived fibrils, and as a result, the hybrid FN network was implemented with a molecular structure similar to that of FN constituting the native ECM of cells.

As with the existing native ECM that makes a scaffold through decellularization (Figure 1h),^[11] it was confirmed whether this hybrid ECM could produce an ECM scaffold through decellularization. Figure 1i shows that the hybrid FN composite network retains the same structure even after the harsh decellularization process. Thus, the hybrid ECM generated by this strategy is very similar to the native ECM in its macroscopic fibril morphology as well as in its protein molecular structure, and can serve as an ideal template that can be utilized for tissue regeneration.

2.2. Hybrid ECM Network Formation

As previously confirmed in Figure 1f, when FN, COL I and LN were added externally to the fibroblast tissue in which the native ECM was formed, a very complex ECM structure was observed. The formula for the relationship between the ECM constituent proteins is not simple; the cFN constituting native ECM can ad-

sorb both pFN and external collagen (exCOL), and it is known that exCOL can also bind to the fibrous COL constituting native ECM. On the other hand, cellular LNs (cLN) do not have any particular interaction with exLN, but unfolded FNs are known to recruit LN binding.^[25] So, in order to figure out how the hybrid ECM will look before the process, it is important to simplify and compare the complex relationships of each component with the native ECM.

We observed structures under confocal microscopy, showing how extrinsically presented proteins alter the structure of the cellular ECM. The single-element depositions (FN, COL I, and LN I) constituting the native ECM were coupled to the cellular ECM as described in the scheme in Figure 2a to build a unique architecture of the hybrid ECM composite. Figure 2b shows z-stack images of the basic architecture of the ECM network before and after adding ECM components. Before adding the ECM component (Figure 2b left), the cFN fibril formed on the FN micropattern showed a branched morphology. In this figure, faint but COL-specific fluorescence was superimposed on the FFNF in white. On a large scale, COL I was discovered as a dispersed blotch. Thus, LN I, denoted by LN $\alpha 1$, was also found to be irregularly scattered in FN and FN patterns (FNp), although very small compared to other ECM components (Figure S2, Supporting Information). The right side of Figure 2b and Movie S1, Supporting Information, are the results of adding all the representative ECM components (FN, COL I, and LN I) to the native ECM. It was observed that the binding of these components to the extracellular membrane resulted in a significant increase in the total amount of ECM.

In order to clearly confirm the position and structural change of each added ECM component, the structure of the native ECM with a single ECM component added was closely observed. In some cases, pFN deposition was confirmed where it was locally formed as separate fibers in the cellular ECM, but in most cases, it was stacked on the cFN as shown in the image and scheme of Figure 2c (Movie S2, Supporting Information). There are known to be intermolecular interactions between the FN–FN binding sites of the FNIII domains that are exposed to the long fibers of cell-based FNs.^[43,45]

Interestingly, exCOL I added to micropatterned fibroblasts builds a unique ECM architecture that completely wraps the fibrous cellular COL I (cCOL I), denoted by COL IA1 (Figure 2d and Movie S3, Supporting Information). The enlarged internal and external 3D shape of the hybrid COL I fibril wrapped with exCOL I can be seen in the confocal microscopy image in Figure 2e. The red fluorescence exCOL I molecules added from the outside completely enveloped the white colored cCOL I fibril in the figure. On the other hand, it is known that FNfs induce COL I synthesis in the periphery, and in fact, hybrid COL I confirmed that the surrounding cFN network coexists. (Figure 2e, rightmost). This study also deposited LN I from mouse Engelbreth–Holm–Swarm (EHS) sarcoma, which consists of $\alpha 1$, $\beta 1$ and $\gamma 1$ heterotrimeric chains into the system.^[46] The newly deposited LN I fibers were placed between FN networks, and cLN I was found as white spots spread across the newly deposited LN I network (Figure S3 and Movie S4, Supporting Information). This is similar to how LN I nanofibers were found in Feinberg and colleagues' study.^[47] Since cLN I molecules have binding sites for various ECM molecules such as nidogens, agrin, perlecan,

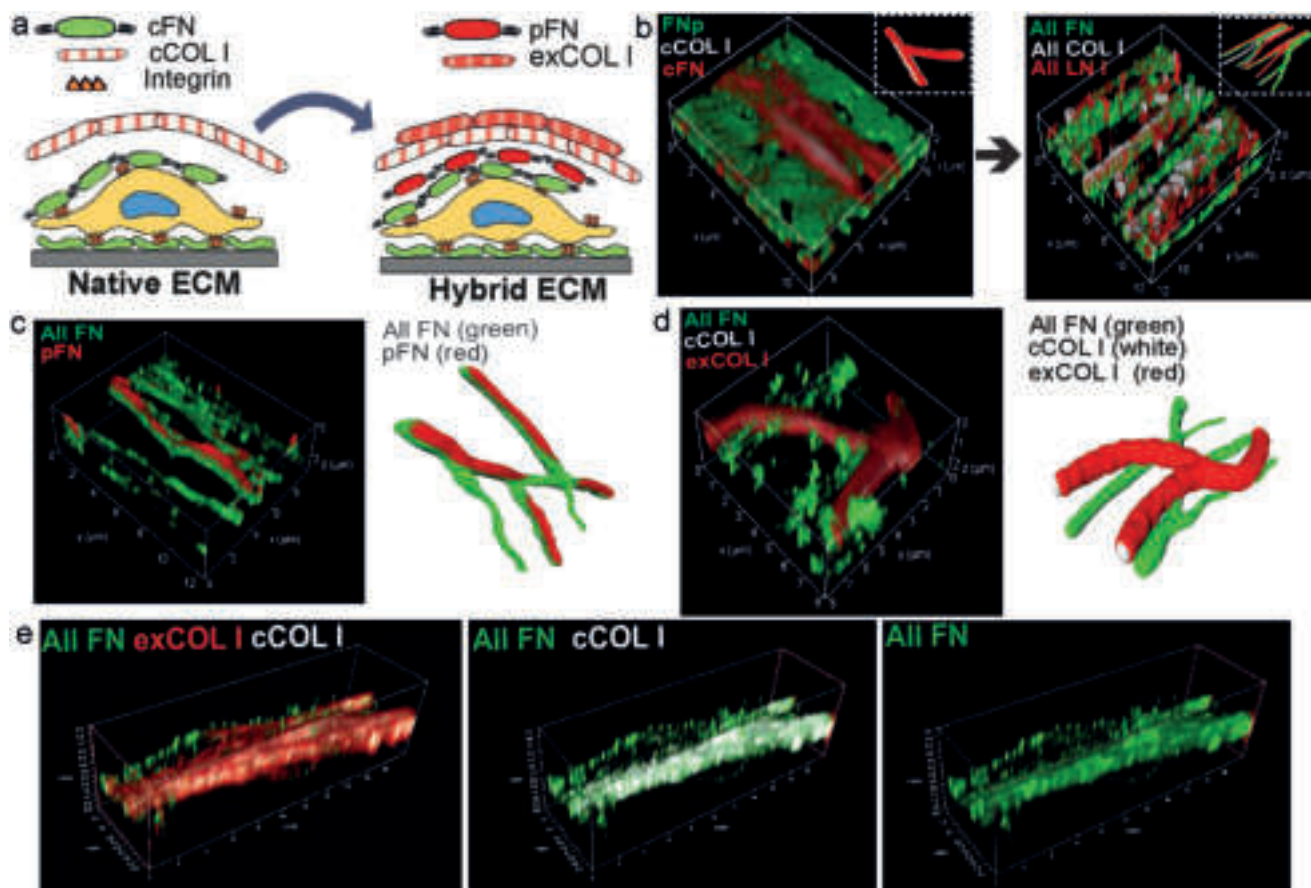


Figure 2. Architecture of various hybrid ECM networks after deposition of external ECM components. a) Schematic of pFN and exCOL I interactions with cFN and cCOL I to generate a hybrid ECM network in micropatterned cells. b) 3D confocal image of the native ECM network (left), with an illustrated model in the dashed box (upper-left) turn into hybrid ECM networks (right), with an illustrated model is shown in the dashed box (upper-right). Confocal images of: c) the hybrid FN network; d) the hybrid COL I network; and e) the enlarged 3D shapes of the hybrid COL I after exCOL I deposition. Full channel of the composite (left), cCOL I and all FN network composite (middle), and all FN network (right). All FN, all COL I and cCOL I networks were detected with antibodies; the pFN and exCOL I were fluorescence labelled.

fibulin-1, heparin and sulfatides,^[46] they are not localized but dispersed on the entire cellular surface. The specific binding of pFN, exCOL I, and exLN I to the native ECM indeed partly affects the morphology and composition of the cellular ECM. However, all external ECM components that constitute a native ECM network are integrated with the cellular ECM, confirming the possibility of realizing a desired ECM composition in a native ECM network.

2.3. Fabrication of Hybrid ECM Networks with Various ECM compositions

We investigated whether it is possible to produce hybrid ECM complex networks with a variety of compositions from a single cellular ECM. We began by depositing varied amounts of exCOL I at concentrations ranging from 0 to 100 $\mu\text{g mL}^{-1}$ onto micropatterned cells. As shown in **Figure 3a**, as the concentration of COL I deposited in the cells increased, hybrid ECMs formed and the intensity of exCOL I in the ECMs increased. A low concentration of exCOL I adsorbed in partial patches onto the cCOL I fibrils, whereas a high concentration of deposited exCOL I fully encir-

led the cCOL I fibers and formed thicker fibers. In addition, adsorption of cFN fibrils exposed to the medium was also observed. At 100 $\mu\text{g mL}^{-1}$, externally administered red COL I coated almost all extracellular fibrils, including cell-induced cCOL I and cFN. As shown in **Figure 3b**, based on the relative fluorescence intensity, the proportion of COL I in the total ECM composition in the control group was $20.09 \pm 2.85\%$ compared to other ECM compositions, and cFN (green) and LN I were $72.13 \pm 4.47\%$ and $7.78 \pm 0.68\%$, respectively. When the concentration of deposited COL I was increased to 12.5, 50 and 100 $\mu\text{g mL}^{-1}$, the proportion of COL I increased to $38.92 \pm 2.105\%$, $87.77 \pm 5.71\%$ and $93.48 \pm 6.06\%$. (**Figure 3b**), indicating that hybrid ECMs of various compositions can be implemented.

Figures 3c,d and 3e,f are confocal and SEM images of hybrid ECM obtained by depositing 50 $\mu\text{g mL}^{-1}$ of COL I and 50 $\mu\text{g mL}^{-1}$ of pFN on fibroblast-derived cellular ECM, respectively. **Figure 3c** shows that 50 $\mu\text{g mL}^{-1}$ of deposited red COL I constitutes a fibril network along the oriented direction of the cells. (Movie S5, Supporting Information). The dense network of COL I-rich ECMs can also be confirmed in the SEM images, forming COL I fibrils with a diameter of $\approx 200\text{--}300$ nm (**Figure 3d**). On the other hand,

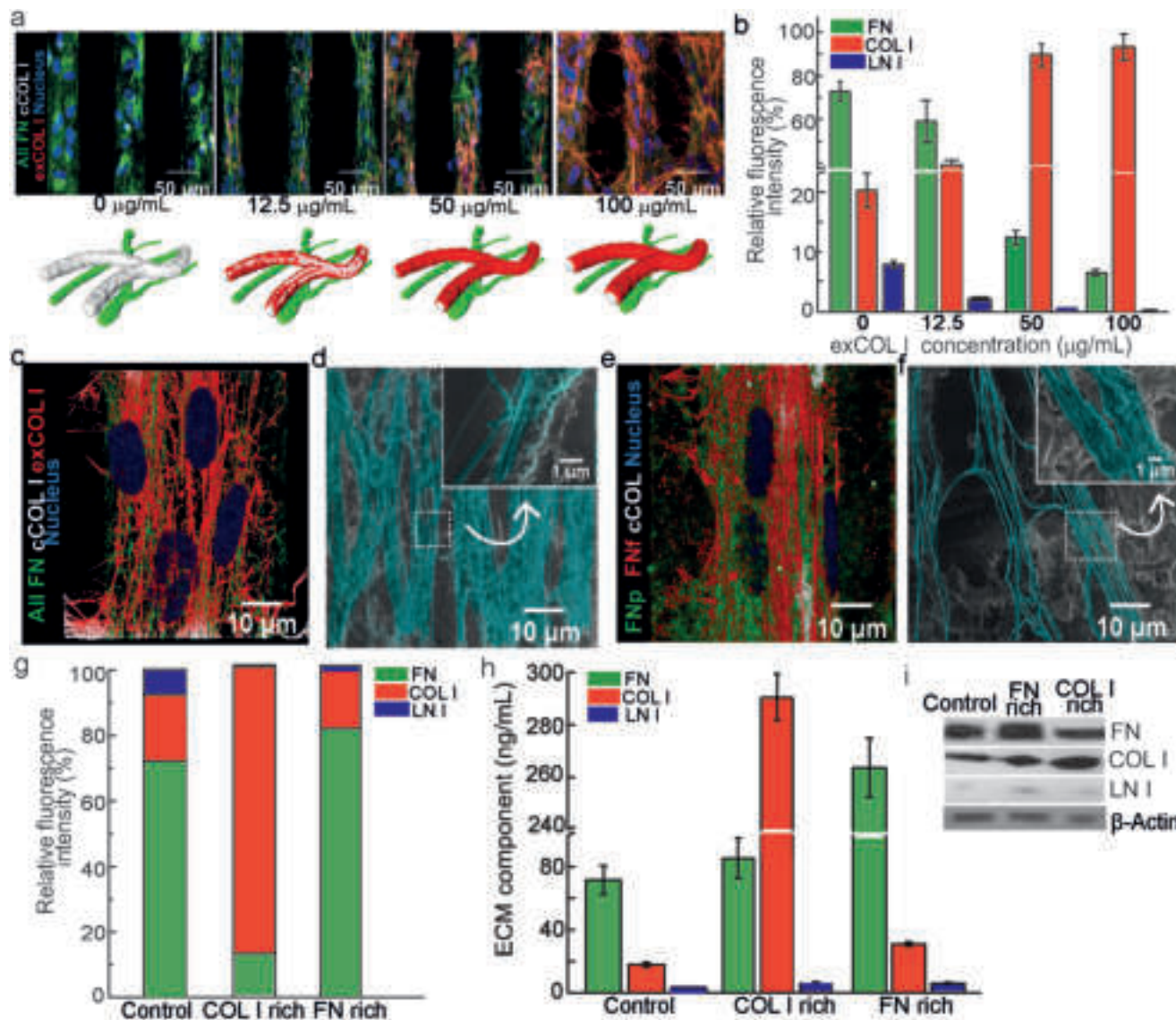


Figure 3. Models for the Fabrication of COL I- and FN-rich ECM composites. a) Confocal microscope images of ECM components for various concentrations of the deposited exCOL I, with illustrated models being shown at the bottom. b) Relative fluorescence intensity of ECM components for various concentrations of deposited exCOL I. COL I-rich ECM networks: c) the confocal image; and d) the SEM images. FN-rich ECM networks: e) the confocal image; and f) the SEM images. In SEM images, the embedded box shows an enlarged image of the dashed area and the blue-green color represents ECM fibers. All FN, FNf, and cCOL I networks were detected with antibodies; the FNp and exCOL I were fluorescence labelled; and nucleus was stained with DAPI. g) Relative fluorescence intensities of the ECM components for COL I-rich and FN-rich ECM; data are means \pm SDs for $n = 3$ experiments. h) Concentrations of the ECM components in the composites, as determined using competitive ELISA; data are means \pm SDs for $n = 3$ experiments. i) Western blot results for the ECM components (FN, COL I and LN I) in the control, the COL I-rich, and the FN-rich composites.

when $50 \mu\text{g mL}^{-1}$ of FN solution was added to the medium, additional FNfs were produced (Figure 3e). A newly formed 100 nm thin fibril was readily observed (Figure 3f), and bundled fiber morphology with a diameter of $\approx 300\text{--}400$ nm, combined with cFN, was also observed (Figure 3e,f and Movie S6, Supporting Information).

While the presence of additionally hybridized ECMs was confirmed by SEM, it was difficult to distinguish the FNp^[48] and cFNs on live fibroblasts nor compositions of ECM types via SEM without selective contrast (Figure S4, Supporting Information). Therefore, confocal microscopy was primarily used to distin-

guish and determine the relative compositions of ECM from the cFN control and hybrid ECM networks, with each being distinguishable by fluorophore-labeled antibodies. Using the composition of cellular ECM constituting fibroblast cells as a control and structural template, the relative compositions of ECM changed to COL I rich and FN rich are shown in Figure 3g. After COL I deposition at a concentration of $50 \mu\text{g mL}^{-1}$, the relative fluorescence intensity of COL I grew rapidly to $86.42 \pm 6.96\%$, whereas FN and LN were 10.26 ± 1.52 and 2.40 ± 0.27 respectively. On the other hand, the addition of FN at a concentration of $50 \mu\text{g mL}^{-1}$ to the same system increased the relative fluorescence intensity of FN

to $81.64 \pm 14.11\%$, whereas the relative fluorescence intensity of COL I and LN I decreased to 18.09 ± 1.34 and $0.26 \pm 0.05\%$, respectively. These results were further quantitatively compared using competition enzyme linked immunosorbent assay (ELISA) (Figure 3h) and Western blot assay (Figure 3i). The quantitative values of each protein in the COL I-rich ECM and FN-rich ECM confirmed essentially the same results as the results observed by the relative fluorescence intensities.

2.4. Decellularization and Recellularization of FN-rich ECM

Most organs are composed of common cell types, such as fibroblast and epithelial cells. While fibroblasts comprise the structural framework of tissues and produce the tissue-specific extracellular matrix, epithelial cells are tightly connected cells arranged with tissue-specific functions in adjacent tissue-specific ECM microenvironments.^[49,50] As an intuitive *in vitro* attempt to fabricate a tissue-specific ECM microenvironment, Figure 4a outlines the experimental procedure to demonstrate an artificial ECM framework that provides a tissue-specific ECM microenvironment. We first constructed a FN-rich model of liver ECM in which fibroblast-derived native ECM was engineered to anchor liver cells; after the FN-rich ECM was prepared, the fibroblasts were decellularized, and hepatocytes were recellularized on the decellularized FN-rich ECM scaffolds.

Indeed, after successfully engineering an FN-rich ECM network on fibroblast cells (Figure 4b), we performed decellularization to remove the cells while preserving the hybrid ECM network (Figure 4c). Figure 4d shows that the composition of the ECM protein is maintained before and after the decellularization process as measured by fluorescence intensity. The efficiency of the decellularization process was assessed by measuring the fluorescence intensity of a nuclear dye via 4',6-diamidino-2-phenylindole dihydrochloride (DAPI), and $\approx 94\%$ of cells were successfully decellularized. (Figure S5, Supporting Information). Liver tissue was selected as a model for FN-rich ECM. Most human tissues are composed primarily of fibrillar collagen, which together with some nonstructural matricellular proteins constitutes the most abundant structural ECM network. On the other hand, liver lobules, unlike other tissues, do not have a basement membrane and are composed of COL I and small amounts of COL III, IV, V and VI, and a greater amount of FN.^[51] As a result, compared to breast-like tissue, where the majority of ECM is made up of COL I molecules, the ECM scaffold for liver tissue regeneration should have a lot more FN molecules, like real liver tissue.^[33] Note that, during the decellularization process of ECM scaffolds, the content of hybrid FNfs was well preserved, whereas hybrid COL components were significantly removed.^[52] Therefore, only recellularization was demonstrated for the decellularized FN-rich ECM composite in this current research.

First, we quantified the number of cell adhesions at an early stage as a cell-biomaterial interaction cascade important for cell proliferation and differentiation. In order to confirm the adhesion of the hepatoma (H4IIE) cells, all samples were prepared in a 50 μm line pattern. As a control for comparison with decellularized FN-rich ECM, the FNp, which is generally used for cell adsorption, and the decellularized cFN of fibroblasts that did not undergo hybridization, were prepared. At initial attachment for

3 and 6 h (Figure 4e), H4IIE cells completely occupied the FN-rich ECM scaffold and FNp control, whereas in the cFN control, H4IIE cells did not fully adhere, or close contact between cells was not made in some parts. Figure 4f shows the density of adsorbed H4IIE cells in the scaffolds of each condition at 3 and 6 h. The number of H4IIE cells per millimeter square on the FN-rich ECM networks was statistically higher than in the FNp or cFN control. We would like to note that cancerous hepatoma cell lines were used in this recellularization experiment, so the results may be slightly different from those using normal hepatocytes. In many other studies, hepatoma cell lines have been also used as liver models,^[53–55] but more accurate comparison experiments with normal hepatocytes should be performed in the future.

At initial attachment for 3 and 6 h, the hepatoma cell density per millimeter square on our FN-rich network (3930.31 ± 680.85) was higher than that on the FNp control (3162.34 ± 653.54) and the cFN control group (2493.56 ± 490.99) ($p < 0.05$). Moreover, after 6 h, our composite network had a statistically higher number of attached cells as shown by the density of $10\,597.82 \pm 1622.84$ cells per millimeter square ($p < 0.01$) while the densities for the FNp and cFN control group were 8510.51 ± 1114.82 and 6501.49 ± 1515.13 cells per millimeter square, respectively (Figure 4f). We can infer that H4IIE cells prefer to adhere to compounds in which exFN is complex with the cellular ECM. These characteristics confirmed that the cells had an initial physicochemical preference for the FN-only control or FN-rich ECM. Therefore, while maintaining the complex fibrillar network structure of ECM derived from cells, it is shown that conversion to a specific preferred surface is possible by converting the surface. At this time, most of the adsorbed H4IIE cells survived on the 5th day, and $94.72 \pm 14.52\%$ of the cells were found to have very high biocompatibility (Figure S6, Supporting Information). It should be noted that when the same fibroblast cells used for the fabrication of cellular ECM were reseeded instead of hepatocytes, there was a statistically similar or slightly higher adhesion density per millimeter square in the cFN (2899.15 ± 439.70 and 5293.51 ± 515.56) scaffold than FNp (2585.97 ± 375.09 and 4429.40 ± 659.54) and FN-rich (2535.36 ± 358.58 and 4429.40 ± 659.54) group both in 3 and 6 h after seeding (Figure 4g and Figure S7, Supporting Information).

3. Conclusion

In this paper, we sought to develop a hybrid ECM scaffold that can be used in a variety of tissues by artificially changing the composition of a natural ECM scaffold. Major ECM proteins such as FN and collagen were supplied from the outside, and it was confirmed that they bind to native ECM derived from cells. While maintaining the basic structure of the natural ECM network provided with native ECM, it was confirmed that the main protein components could be regulated through this method. We then proceeded with decellularization to create hybrid ECM scaffolds with altered protein composition. In addition, it was confirmed that the decellularized hybrid ECM provides a specialized microenvironment required for other organs or tissues, and can successfully settle cells derived from other tissues. Although it was not yet possible to fully replicate the complex biological properties of a specific organ, we believe that this ECM platform can be

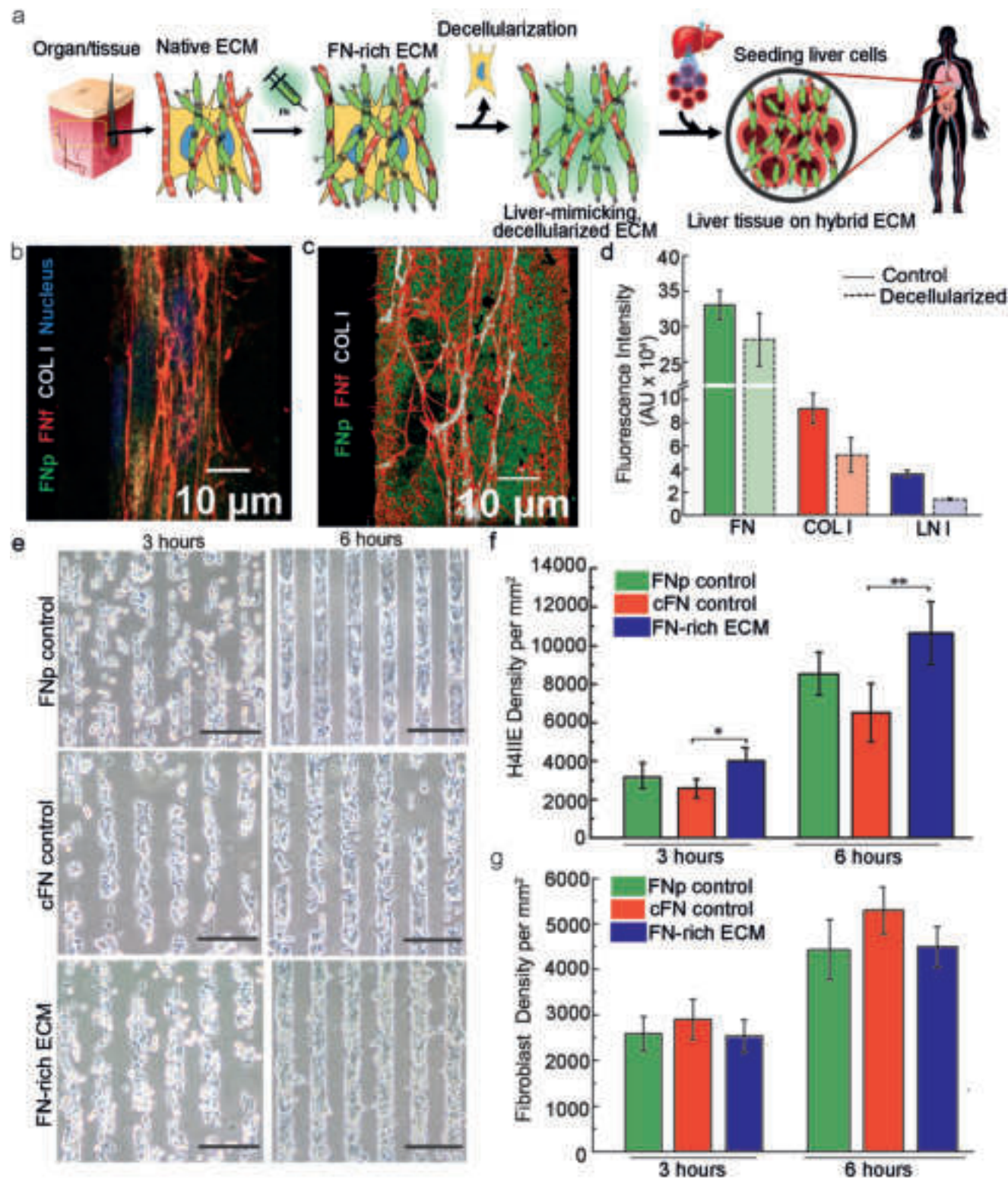


Figure 4. Decellularization and recellularization of FN-rich ECM composites. a) Scheme for the fabrication, decellularization and recellularization of an FN-rich ECM composite. Confocal images of FN rich-ECM: b) before decellularization, and c) after decellularization. FNf and cCOL I were detected with antibodies; the FNp was fluorescence labelled; and nucleus was stained in DAPI. d) Fluorescence intensity of the retained ECM network; data are means \pm SDs for $n = 3$ experiments. e) Recellularization of the FN-rich ECM composite with H4IIE cells at 3 and 6 h; scale bars represent 150 μ m. f) H4IIE cell density on the composite at 3 and 6 h; data are means \pm SDs for $n = 4$ experiments. Statistical significance was determined using the one-way ANOVA followed by the Tukey test; $*p < 0.05$. g) Fibroblast cell density on the composite at 3 and 6 h; data are means \pm SDs for $n = 3$ experiments.

a promising method that is universally applicable to promote the repair or regeneration of damaged organs in tissue engineering.

4. Experimental Section

Materials and Reagents: The base and the curing agent for the silicone elastomer were supplied by Sylgard 184 (Dow Corning). Glutaraldehyde (GA) (G5882), (3-aminopropyl) triethoxysilane (APTES) (440 140), Triton-X 100, 4',6-diaminodino-2-phenylindole (DAPI), paraformaldehyde (P6148), Tween 20 (P1754), and bovine serum albumin (BSA) (A9647) were procured from Sigma-Aldrich. Human plasma fibronectin was purchased from Invitrogen (33 016 015) while rat tail and bovine collagen I were purchased from Gibco (A1048301 and A1064401). Mouse EHS was procured from Sigma (11 243 217 001). The phosphate buffer saline (PBS) (10010-023) used in this research, and trypsin-EDTA in the cell culture were purchased from Gibco. Cells were maintained in Dulbecco's Minimum Essential Media (DMEM, Gibco 11 995 065) containing 10% fetal bovine serum (FBS, Gibco 16 000 044), and 1% penicillin-streptomycin-glutamine 100× (Gibco, 10 378 016). The ECM (FN/COL I/ LN I) fluorescent dyes, succinimidyl (NHS) ester of Alexa Fluor 488 (A2000), succinimidyl (NHS) ester of Alexa Fluor 647 and Alexa Fluor C5 maleimide (A10258), were supplied by Life Technologies. The primary antibodies used in this study for immunocytochemistry were rabbit anti-fibronectin (Sigma Aldrich, F3648), rat polyclonal anti-LN α 1 (Abcam, 2466), and mouse collagen type 1A (Santa Cruz, 59 772). On the other hand, the polyclonal COL I (NB600-408), and LN (PA1-163730) antibodies for ELISA were purchased from Novus Bio and Invitrogen, respectively. Furthermore, the secondary antibodies for immunocytochemistry were anti-rabbit Alexa Fluor 488 (Invitrogen, MOP-A11034) for FN visualization, while anti-mouse Alexa Fluor 568 (Invitrogen, MOP-A21124), and anti-mouse Alexa Fluor 647 (Invitrogen, A23728) for detecting cCOL I and cLN I. Additionally, nucleus was stained with DAPI (Sigma, D9542). The secondary antibody for ELISA, horseradish peroxidase conjugated goat anti-rabbit IgG-HRP (ab6721), was purchased from Abcam. Cell culture dishes and pipettes were purchased from SPL Life Sciences. For protein extraction, RIPA buffer (89 900), protease and phosphatase inhibitors (78 425 and 78 420) purchased from Thermo Scientific were used. Thiourea (T8656), urea (36 428), tris base (252 859), dithiothreitol (1 097 777 001), and sodium dodecyl sulfate (L3771) were purchased from Sigma-Aldrich. For the western blot test, the Pierce modified Lowry (P1856006) method of Thermo Fischer Scientific was used.

ECM Microcontact Printing Technique: The patterned silicon wafer was generated using a well-established soft lithography process.^[48,56] The thin stamp technique produced PDMS stamps by mixing the base, and the curing agent of Sylgard 184 in a 10:1 ratio, and the mixture was poured into a patterned wafer, as mentioned in the authors' previous study.^[48] After degassing, the stamps were set at 65 °C for 4 h; then, they were cut out from the silicon master in 20 mm × 20 mm pieces. In this study, a pattern of 50- μ m lines was used. For the microcontact printing (μ CP) substrate, PDMS at the same ratio as was used to produce the stamp was spin-coated onto cleaned coverslips. The PDMS-coated coverslips were further cured, as previously mentioned. Before the stamping process, the surface of PDMS was chemically activated using the method of Kuddannaya et al. (2013) by immersing it in 10% APTES in distilled water at 50 °C for 2 h and then washing it with deionized (DI) water three times. This substrate was then incubated in a 2.5% GA solution in DI water at room temperature (RT) for an hour, washed with DI water three times, and then dried in an oven.^[34]

The ink for μ CP was prepared using fluorescence labelling of fibronectin with excessive molar NHS Alexa 488, and it was allowed to sit for an hour at RT in a PBS (0.1 M HCL) solution. Excess fluorescence dye was removed using PD Spintrap G-25. The labelled protein was kept at 4 °C until it was used. The PDMS stamp was immersed in labelled FN at a concentration 50 μ g mL⁻¹ in PBS for an hour at RT, after which the solution was removed from the PDMS stamp and dried under N₂. The protein transfer from the stamp to the substrate was achieved by pressing the stamp gently on the surface of the activated substrate. In the noncellular control, Figure 1c, FN

micropattern was labelled using NHS Alexa 488, while deposited pFN was labelled using NHS Alexa 647. In the basic study, as shown in Figure 1e,f, after FN microcontact printing, the FN patterns with excess primary rabbit anti-fibronectin (Sigma Aldrich, F3648) and goat anti-rabbit IgG-HRP (ab6721) were blocked so that those patterns would not be detected by immunostaining. The microcontact printed PDMS was then transferred into 35-mm cell dishes and blocked with 2% BSA solution in PBS for an hour at RT or overnight at 4 °C. The excess BSA solution was removed; then, the dishes were washed with PBS, sterilized and kept in PBS solution at 4 °C until use.

Cell Seeding and Hybrid ECM Fabrication: Normal human dermal fibroblast (NHDF) cells at passages 4 to 12 were maintained in DMEM with 10% FBS and 1% antibiotics at 37 °C in a 5% CO₂ incubator until they had reached a confluent state. Normal human dermal fibroblast (NHDF) cells were washed using PBS and detached enzymatically using trypsin-EDTA (0.25%) during the subculture. The cells were collected in a 15-mL conical tube by centrifugation (Eppendorf 5810R) at 1500 rpm for 3 min. The media were removed, after which the cell pellets were suspended in DMEM with 2.5% FBS and 1% antibiotics. The cell numbers were calculated before conducting further experiments. Several samples with 10⁶ cells/mL in DMEM containing low serum (2.5% FBS) were added to the patterned coverslips that had been prepared previously. After 3 h, ECM containing low serum media was changed to remove unbound cells, and the cells were continuously grown for 24 h. For studying the architecture of hybrid ECM, a single red fluorescing component was added, labelled 50 μ g mL⁻¹ human plasma FN/bovine COL I/mouse EHS LN I, to the micropatterned cells in a low serum medium (2.5% FBS). Then, with the exception of the sample with added COL I, which had been grown for 4 h, the micropatterned cells were continuously grown for 24 h. The multicomponent ECM combinations were built by depositing a combination of human plasma FN, rat tail COL I and EHS LN I in the same concentration (25 μ g mL⁻¹) in a low serum medium (2.5% FBS), which was then added to the cells and continuously grown for 24 h. For titrating the micropatterned cells, red-fluorescing labelled-bovine COL I solutions at concentrations of 0, 12.5, 50 and 100 μ g mL⁻¹ in low serum media were added. For the fabrication of the COL I-rich and the FN-rich ECM networks, 50 μ g mL⁻¹ of COL I and FN were used.

Immunocytochemistry: The cells were fixed in 4% buffered paraformaldehyde for 20 min^[57]. The fixed cells were washed two times with PBS for 5 min each time, followed by 0.1% Triton-X 100 in TBS for 3 min. The samples were blocked using a 2% BSA solution in PBS for an hour at RT or overnight at 4 °C in order to eliminate unspecific binding of the primary antibody. After the samples had been blocked, they were incubated with primary antibody for an hour at RT. Unbound antibodies were further washed away with TBS solution containing 0.1% Tween (TBST) three times for 15 min each time. The cells were incubated with secondary antibodies with or without DAPI for an hour. Excessive antibodies were removed by washing three times for 15 min each time. The coverslips were mounted in deck glass before confocal Leica SP-8 microscope imaging. For quantitative analysis, the experiments were set up at the same intensity level for each channel: 16 frame and 4 line average, 1 line and 1 frame accumulation.

SEM Imaging: The cells on PDMS-coated coverslips from a previous experiment were immersed in 4% buffered paraformaldehyde for 20 min and were then gently washed three times for an hour each time with distilled water to remove salt. The samples were dried at 37 °C overnight, were fixed on a silicon wafer, and were then observed using Zeiss JSM-7100F system.

Fluorescence Resonance Energy Transfer (FRET) Analysis: Fibronectin (FN) at not less than 2 mg mL⁻¹ was labelled with Alexa NHS 488 and Alexa C5 maleimide 546, as modified by Smith et al. (2007).^[58,59] Briefly, 8-m guanidine hydrochloride (Gdn HCl) in NaHCO₃ buffer at pH 8.5 was added to the FN solution for 15 min to open its molecular structure. FN was first labelled with 20-fold excess acceptor Alexa C5 maleimide for 3 h at RT or overnight at 4 °C. Labelled proteins were dialyzed against NaHCO₃ buffer two times for 3 h each time and overnight at 4 °C to remove the excess dye. Furthermore, FN was labeled with 60-fold excess donor Alexa NHS 488 for 2 h. Double-labelled FN, further named

FN-donor acceptor (FN-DA), was separated from excess dye by using a PD-column that had previously been equilibrated with PBS. The FN-DA was kept in a solution with a 10% glycerol concentration at -20°C until use. The FRET efficiency was determined by using the photobleaching method with a SP-8 Leica confocal microscope. To demonstrate FRET efficiency titration of the FN secondary structure, various concentrations of Gdn HCl (0–6 M) were added to the FN-DA solution and then fixed it in a 1% agarose solution. The FRET efficiency was calculated by using the photobleaching method with LAS-X software at ten different points in every sample from four different independent experiments. For FN fibrillogenesis on micropatterned ECM, unlabeled ECM solution was used as the ink for microcontact printing for which the detailed process was mentioned previously. After the stamping process, the PDMS substrate was transferred into a culture dish, blocked with 2% BSA and sterilized. Cells at a concentration of 1×10^6 cells/mL in low serum DMEM were deposited on the PDMS substrate. After the cells had attached themselves to the ECM micropattern, the medium was changed into a FRET FN-containing medium and was continuously cultured. After 24 h, the cells were fixed and then observed under a confocal SP-8 microscope to determine the FRET efficiency by using the photobleaching acceptor method.

Protein Extraction and Western Blot: Protein extraction from cells was done based on Ngoka's study.^[60] After the hybrid ECM had been grown, as previously mentioned, cells were scrapped in 250 μL of cold RIPA buffer and then agitated for 30 min. To increase the yield of extracted protein, cell lysates were sonicated every 5 min, collected the lysate in microtubes and then centrifuged at 10 000 g at 4°C for 20 min. The supernatant was collected, and remaining pellets were extracted using 100 μL of urea buffer consisting of 5-M urea, 2-M thiourea, 50-mM DTT and 0.1% SDS in tris base to dissolve fibronectin at 4°C , were agitated, and were then centrifuged at 14 000 rpm for 20 min. The supernatant was added to the previous supernatant and used for determining the protein concentration by using the Pierce™ modified Lowry method according to manufacturer's instruction. Briefly, 40 μL of sample and BSA standard solutions were added into a 96-well plate and mixed thoroughly on a plate shaker for 10 min. Then, 20 μL of Folin–Ciocalteu reagent was mixed into each well and shaken for 30 s. The 96-well plate was incubated at RT for 30 min while being protected from light. The absorbance of the reaction product was measured at a 750-nm wavelength (Enspire, PerkinElmer). The extracted proteins were separated using sodium dodecyl sulfate-polyacrylamide gel electrophoresis (SDS-PAGE) with 10% acrylamide and were then transferred to polyvinylidene fluoride (PVDF) membranes. Next, a blocking process was performed with 5% skim milk (non-fat), and the membrane was washed with TBST three times for 15 min each time. The blocked membrane was then incubated with primary antibodies, as previously mentioned, in a 1:400 dilution overnight at 4°C . After the membrane had been washed, horseradish peroxidase-linked secondary antibody was used for colorimetric detection.

ECM Components Quantification: The ECM components of each composite were quantified using ELISAs that had been modified in accordance with the study by Rennard and colleagues.^[61] A 96-well plate was coated with $1 \mu\text{g mL}^{-1}$ of FN/LN I/COL I in 0.1% BSA in TBS as a coating buffer and was maintained overnight at a temperature of 4°C . The remaining proteins were washed away in tris buffered saline and Tween-20 (TBST). The coated plate was blocked with 1% BSA in TBS for an hour at RT, after which it was washed with TBST three times to remove unbound BSA from the bottom plate. Simultaneously, the samples were prepared by incubating, for an hour at RT, 50 μL of standard or sample in 50 μL of anti-FN/COL I/LN I antibody (1:10 000) isolated from rabbits. After the blocking process had been completed, 100 μL of prepared sample was added to the well plate and incubated for an hour at RT. After the remaining antibody had been washed with TBST three times, secondary antibody mouse anti-rabbit IgG-HRP was added to each well and incubated for an hour at RT. After the excess antibody had been washed away three times with TBST at RT, 100 μL of the tetramethylbenzidine (TMB) substrate was added to each well and incubated for 30 min. The complex products were dissolved in 1-M HCl, and the absorbance was measured at a wavelength of 450 nm by using a multi-plate reader (EnSpire, Perkin Elmer).

Decellularization and Recellularization: ECM hybrid composites were grown as previously mentioned. The cells were removed from the composite by washing it with 25-mM NH_4OH for 20 min.^[62] The composite was washed with PBS and then blocked using 2% BSA for an hour or overnight. FN-rich composites were recellularized using H4IIE rat hepatoma cells maintained in Eagle MEM with non-essential amino acids and Earle's BSS with 10% FBS, 10% calf serum, and 1% penicillin-streptomycin. The number of attached cells was observed at 3 and 6 h. The assessments of dead and live cells were accomplished on days 0, 1, 3, and 5 by using the double staining method based on a previous study.^[63]

Image Analysis: The images were analyzed using Image J software and the LASX program. The fluorescence intensity was obtained from Image J normalized to the background intensity from every stack while Z-projected images were visualized in the LASX program. The FRET efficiency was analyzed using FRET-AB in a SP-8 confocal microscope from Leica.

Statistical Analysis: All data were preprocessed to identify outliers, after which data were presented as means \pm standard deviations (SDs) from at least three independent measurements. Data were analyzed using the one-way ANOVA followed by Tukey's test, and the level of significance was determined at $*p < 0.05$ by using Origin 9.0.

Supporting Information

Supporting Information is available from the Wiley Online Library or from the author.

Acknowledgements

This work was supported by the Basic Research Program (2018R1A6A1A03024940) of the Ministry of Education, the Mid-Career Researcher Program (2019R1A2C2084638) and the Global Research Network Program (2021K1A4A8A02079222) of the Ministry of Science and ICT, Korea. A.S received the Korean Government's Scholarship Program for Doctoral Degree (KGSP-GRA-2016-263) and S.L. received the Scholarship from the Training program of CCUS for the green growth (2021A000000500) of Korea Institute of Energy Technology Evaluation and Planning.

Conflict of Interest

The authors declare no conflict of interest.

Data Availability Statement

The data that support the findings of this study are available in the supplementary material of this article.

Keywords

collagen, extracellular matrix, fibronectin, laminin, tissue engineering

Received: March 11, 2022

Revised: May 24, 2022

Published online: July 15, 2022

[1] J. Winkler, A. Abisoye-Ogunniyan, K. J. Metcalf, Z. Werb, *Nat. Commun.* **2020**, *11*, 5120.

[2] C. Bonnans, J. Chou, Z. Werb, *Nat. Rev. Mol. Cell Biol.* **2014**, *15*, 786.

- [3] M. C. Ratri, A. I. Brilian, A. Setiawati, H. T. Nguyen, V. Soum, K. Shin, *Adv. NanoBiomed Res.* **2021**, *1*, 2000088.
- [4] X. Cun, L. Hosta-Rigau, *Nanomaterials* **2020**, *10*, 2070.
- [5] A. V. Shinde, N. G. Frangogiannis, *Curr. Pathobiol. Rep.* **2017**, *5*, 145.
- [6] M. D'Urso, N. A. Kurniawan, *Front. Bioeng. Biotechnol.* **2020**, *8*, 609653.
- [7] A. V. Shinde, N. G. Frangogiannis, *J. Mol. Cell. Cardiol.* **2014**, *70*, 74.
- [8] S. Battista, D. Guarnieri, C. Borselli, S. Zeppetelli, A. Borzacchiello, L. Mayol, D. Gerbasio, D. R. Keene, L. Ambrosio, P. A. Netti, *Biomaterials* **2005**, *26*, 6194.
- [9] L. Krishna, K. Dhamodaran, C. Jayadev, K. Chatterjee, R. Shetty, S. S. Khora, D. Das, *Stem Cell Res. Ther.* **2016**, *7*, 188.
- [10] P. E. Bourguine, B. E. Pippenger, A. Todorov, L. Tchang, I. Martin, *Biomaterials* **2013**, *34*, 6099.
- [11] T. Hoshiba, G. Chen, C. Endo, H. Maruyama, M. Wakui, E. Nemoto, N. Kawazoe, M. Tanaka, *Stem Cells Int.* **2016**, *2016*, 6397820.
- [12] A. Setiawati, H. T. Nguyen, Y. Jung, K. Shin, *Int. Neurolog. J.* **2018**, *22*, S66.
- [13] G. Rijal, W. Li, *Sci. Adv.* **2017**, *3*, e1700764.
- [14] Y. Guan, S. Liu, C. Sun, G. Cheng, F. Kong, Y. Luan, X. Xie, S. Zhao, D. Zhang, J. Wang, K. Li, Y. Liu, *Oncotarget* **2015**, *6*, 36126.
- [15] A. S. Mao, D. J. Mooney, *Proc. Natl. Acad. Sci. USA* **2015**, *112*, 14452.
- [16] S. Petrus-Reurer, M. Romano, S. Howlett, J. L. Jones, G. Lombardi, K. Saeb-Parsy, *Commun. Biol.* **2021**, *4*, 798.
- [17] R. Yoshimi, H. Nakajima, *Front. Med.* **2022**, *9*, 813952.
- [18] S. Ahn, L. F. Deravi, S.-J. Park, B. E. Dabiri, J.-S. Kim, K. K. Parker, K. Shin, *Adv. Mater.* **2015**, *27*, 2838.
- [19] L. A. Sawicki, E. M. Ovidia, L. Pradhan, J. E. Cowart, K. E. Ross, C. H. Wu, A. M. Kloxin, *APL Bioeng.* **2019**, *3*, 016101.
- [20] J. Liu, H. Long, D. Zeuschner, A. F. B. Räder, W. J. Polacheck, H. Kessler, L. Sorokin, B. Trappmann, *Nat. Comm.* **2021**, *12*, 3402.
- [21] L. Yang, H. Wu, L. Lu, Q. He, B. Xi, H. Yu, R. Luo, Y. Wang, X. Zhang, *Biomaterials* **2021**, *276*, 121055.
- [22] K. S. Hellmund, B. Lospichl, C. Böttcher, K. Ludwig, U. Keiderling, L. Noirez, A. Weiß, D. J. Mikolajczak, M. Gradzielski, B. Kokschi, *Pept. Sci.* **2021**, *113*, e24201.
- [23] C. Licht, J. C. Rose, A. O. Anarkoli, D. Blondel, M. Roccio, T. Haraszti, D. B. Gehlen, J. A. Hubbell, M. P. Lutolf, L. De Laporte, *Biomacromolecules* **2019**, *20*, 4075.
- [24] C. D. Cook, A. S. Hill, M. Guo, L. Stockdale, J. P. Papps, K. B. Isaacson, D. A. Lauffenburger, L. G. Griffith, *Integr. Biol.* **2017**, *9*, 271.
- [25] S. Ahn, K. Y. Lee, K. K. Parker, K. Shin, *Sci. Rep.* **2018**, *8*, 1913.
- [26] W. S. To, K. S. Midwood, *Fibrog. Tissue Repair* **2011**, *4*, 21.
- [27] D. F. Mosher, R. B. Johnson, *J. Biol. Chem.* **1983**, *258*, 6595.
- [28] K. Sakai, T. Fujii, T. Hayashi, *J. Biochem.* **1996**, *119*, 58.
- [29] N. Pernodet, M. Rafailovich, J. Sokolov, D. Xu, N. L. Yang, K. Mcleod, *J. Biomed. Mater. Res., Part A* **2003**, *64A*, 684.
- [30] J. A. Paten, C. L. Martin, J. T. Wanis, S. M. Siadat, A. M. Figueroa-Navedo, J. W. Ruberti, L. F. Deravi, *Chem* **2019**, *5*, 2126.
- [31] K. Scheuer, C. Helbing, I. Firkowska-Boden, K. D. Jandt, *RSC Adv.* **2021**, *11*, 14113.
- [32] D. B. Neale, A. J. Muñiz, M. S. Jones, D. H. Kim, J. M. Buschhaus, B. A. Humphries, W. Y. Wang, B. M. Baker, J. E. Raymond, L. Solorio, G. D. Luker, J. Lahann, *Small Struct.* **2021**, *2*, 2000137.
- [33] E. T. Goddard, R. C. Hill, A. Barrett, C. Betts, Q. Guo, O. Maller, V. F. Borges, K. C. Hansen, P. Schedin, *Int. J. Biochem. Cell Biol.* **2016**, *81*, 223.
- [34] S. Kuddannaya, Y. J. Chuah, M. H. A. Lee, N. V. Menon, Y. Kang, Y. Zhang, *ACS Appl. Mater. Interfaces* **2013**, *5*, 9777.
- [35] A. W. Feinberg, K. K. Parker, *Nano Lett.* **2010**, *10*, 2184.
- [36] T. Pompe, L. Renner, C. Werner, *Biophys. J.* **2005**, *88*, 527.
- [37] S. M. Früh, I. Schoen, J. Ries, V. Vogel, *Nat. Commun.* **2015**, *6*, 7275.
- [38] C. Zhong, M. Chrzanowska-Wodnicka, J. Brown, A. Shaub, A. M. Belkin, K. Burridge, *J. Cell Biol.* **1998**, *141*, 539.
- [39] D. D. Schlaepfer, M. A. Broome, T. Hunter, *Mol. Cell. Biol.* **1997**, *17*, 1702.
- [40] S. K. Mitra, D. A. Hanson, D. D. Schlaepfer, *Nat. Rev. Mol. Cell Biol.* **2005**, *6*, 56.
- [41] T. Velling, J. Risteli, K. Wennerberg, D. F. Mosher, S. Johansson, *J. Biol. Chem.* **2002**, *277*, 37377.
- [42] S. Li, C. Van Den Diepstraten, S. J. D'souza, B. M. C. Chan, J. G. Pickering, *Am. J. Pathol.* **2003**, *163*, 1045.
- [43] J. Graham, M. Raghunath, V. Vogel, *Biomater. Sci.* **2019**, *7*, 4519.
- [44] J. M. Szymanski, K. Zhang, A. W. Feinberg, *Sci. Rep.* **2017**, *7*, 13413.
- [45] Y. Mao, J. E. Schwarzbauer, *Matrix Biol.* **2005**, *24*, 389.
- [46] M. Durbeej, *Cell Tissue Res.* **2010**, *339*, 259.
- [47] J. M. Szymanski, M. Ba, A. W. Feinberg, *J. Mater. Chem. B* **2015**, *3*, 7993.
- [48] H. Ko, L. F. Deravi, S. J. Park, J. Jang, T. Lee, C. Kang, J. S. Lee, K. K. Parker, K. Shin, *Adv. Mater.* **2017**, *29*, 1701732.
- [49] P. Mallinoud, J. P. Villemain, H. Mortada, M. P. Espinoza, F. O. Desmet, S. Samaan, E. Chautard, L. C. Tranchevent, D. Aubeuf, *Genome Res.* **2014**, *24*, 511.
- [50] L. E. Tracy, R. A. Minasian, E. J. Caterson, *Adv. Wound Care* **2016**, *5*, 119.
- [51] A. Martinez-Hernandez, P. S. Amenta, *Virchows Arch. A: Pathol. Anat. Histopathol.* **1993**, *423*, 1.
- [52] Q. Shi, C. Chen, M. Li, Y. Chen, Y. Xu, J. Hu, J. Liu, H. Lu, *BMC Musculoskeletal Disord.* **2021**, *22*, 235.
- [53] C. T. Ho, R. Z. Lin, R. J. Chen, C. K. Chin, S. E. Gong, H. Y. Chang, H. L. Peng, L. Hsu, T. R. Yew, S. F. Chang, C. H. Liu, *Lab Chip* **2013**, *13*, 3578.
- [54] V. Hosseini, N. F. Maroufi, S. Saghati, N. Asadi, M. Darabi, S. N. S. Ahmad, H. Hosseinkhani, R. Rahbarghazi, *J. Transl. Med.* **2019**, *17*, 383.
- [55] Y. Wang, M. H. Kim, H. Shirahama, J. H. Lee, S. S. Ng, J. S. Glenn, N. J. Cho, *Sci. Rep.* **2016**, *6*, 37427.
- [56] J. F. Ashley, N. B. Cramer, R. H. Davis, C. N. Bowman, *Lab Chip* **2011**, *11*, 2772.
- [57] V. Guneta, Z. Zhou, N. S. Tan, S. Sugii, M. T. C. Wong, C. Choong, *Biomater. Sci.* **2018**, *6*, 168.
- [58] M. L. Smith, D. Gourdon, W. C. Little, K. E. Kubow, R. A. Eguiluz, S. Luna-Morris, V. Vogel, *PLoS Biol.* **2007**, *5*, 2243.
- [59] J. S. Nanda, J. R. Lorsch, *Methods in Enzymology* (Eds: J. Lorsch), vol. 536, Academic Press, San Diego **2014**, Ch. 7.
- [60] L. C. M. Ngoka, *Proteome Sci.* **2008**, *6*, 30.
- [61] S. I. Rennard, R. Berg, G. R. Martin, J. M. Foidart, P. G. Robey, *Anal. Biochem.* **1980**, *104*, 205.
- [62] H. Lu, T. Hoshiba, N. Kawazoe, G. Chen, *J. Biomed. Mater. Res., Part A* **2012**, *100A*, 2507.
- [63] J. H. Choi, A. Park, W. Lee, J. Youn, M. A. Rim, W. Kim, N. Kim, J. E. Song, G. Khang, *J. Controlled Release* **2020**, *327*, 747.